



Ferromagnetism induced by lattice volume expansion and  
amorphization in EuTiO<sub>3</sub> thin film

Journal:	Journal of Materials Research
Manuscript ID:	JMR-2012-0621.R2
Manuscript Type:	Invited Feature Paper
Date Submitted by the Author:	n/a
Complete List of Authors:	Tanaka, Katsuhisa; Kyoto University, Department of Material Chemistry, Graduate School of Engineering Fujita, Koji; Kyoto University, Department of Material Chemistry, Graduate School of Engineering Maruyama, Yuya; Kyoto University, Department of Material Chemistry, Graduate School of Engineering Kususe, Yoshiro; Kyoto University, Department of Material Chemistry, Graduate School of Engineering Murakami, Hideo; Kyoto University, Department of Material Chemistry, Graduate School of Engineering Akamatsu, Hirofumi; Kyoto University, Department of Materials Science and Engineering, Graduate School of Engineering Zong, Yanhua; Kyoto University, Department of Material Chemistry, Graduate School of Engineering Murai, Shunsuke; Kyoto University, Department of Material Chemistry, Graduate School of Engineering
Key Words:	ferromagnetic, oxide, thin film

1  
2  
3  
4  
5  
6 Ferromagnetism induced by lattice volume expansion and amorphization in  $\text{EuTiO}_3$  thin  
7  
8 film  
9

10  
11  
12  
13 Katsuhisa Tanaka<sup>1</sup>, Koji Fujita<sup>1</sup>, Yuya Maruyama<sup>1</sup>, Yoshiro Kususe<sup>1</sup>, Hideo Murakami<sup>1</sup>,  
14  
15 Hirofumi Akamatsu<sup>2</sup>, Yanhua Zong<sup>1</sup>, and Shunsuke Murai<sup>1</sup>  
16

17  
18  
19  
20 1 Department of Material Chemistry, Graduate School of Engineering, Kyoto University,  
21  
22 Katsura, Nishikyo-ku, Kyoto 615-8510, Japan  
23

24  
25 2 Department of Materials Science and Engineering, Graduate School of Engineering, Kyoto  
26  
27 University, Yoshida-honmachi, Sakyo-ku, Kyoto 606-8501, Japan  
28

29  
30  
31  
32 Corresponding author: Katsuhisa Tanaka, [tanaka@dipole7.kuic.kyoto-u.ac.jp](mailto:tanaka@dipole7.kuic.kyoto-u.ac.jp)  
33  
34  
35  
36  
37  
38  
39  
40  
41  
42  
43  
44  
45  
46  
47  
48  
49  
50  
51  
52  
53  
54  
55  
56  
57  
58  
59  
60

1  
2  
3  
4  
5  
6 Abstract  
7

8 The lattice volume expansion or amorphization renders  $\text{EuTiO}_3$  ferromagnetic although  
9 the stable phase of crystalline  $\text{EuTiO}_3$  is an antiferromagnet. The lattice volume expansion is  
10 induced into crystalline  $\text{EuTiO}_3$  thin film by utilizing the lattice mismatch between the thin film  
11 and a substrate. The magnetization at low temperatures monotonically increases with an  
12 increase in lattice volume for the crystalline  $\text{EuTiO}_3$  thin film, coincident with the results of  
13 calculations based on hybrid Hartree-Fock density functional approach. The ferromagnetic  
14 interaction between  $\text{Eu}^{2+}$  ions is enhanced by the amorphization as well; amorphous  $\text{EuTiO}_3$  thin  
15 film becomes a ferromagnet, and the Curie temperature is higher for amorphous  $\text{Eu}_2\text{TiO}_4$  than  
16 for its crystalline counterpart. The phenomenon, that is, the volume expansion- and  
17 amorphization-induced ferromagnetism, is explained in terms of the competition between  
18 ferromagnetic and antiferromagnetic interactions among  $\text{Eu}^{2+}$  ions; the former stems from the  
19 indirect exchange interaction via  $\text{Eu}^{2+}$  5d state and the latter is caused by the superexchange  
20 interaction via  $\text{Ti}^{4+}$  3d state.  
21  
22  
23  
24  
25  
26  
27  
28  
29  
30  
31  
32  
33  
34  
35  
36  
37  
38  
39  
40  
41  
42  
43  
44  
45  
46  
47  
48  
49  
50  
51  
52  
53  
54  
55  
56  
57  
58  
59  
60

## I. INTRODUCTION

Considerable attention has been paid to oxides containing transition metal elements for the last several decades from a point of view of their unique electronic structures and curious physical properties including electrical conduction, dielectric properties, magnetism, and optical properties. Among many sorts of oxide, those having perovskite and its related structures, in particular, exhibit intriguing electrical and magnetic properties. One of the prototypes of properties the oxides with perovskite structure manifest is ferroelectricity. Several kinds of oxide such as  $\text{BaTiO}_3$ ,  $\text{Pb}(\text{Zr,Ti})\text{O}_3$ ,  $(\text{Pb,Lu})(\text{Zr,Ti})\text{O}_3$ , and  $\text{KNbO}_3$  are ferroelectric at room temperature, and they are practically utilized as capacitors, piezoelectric devices, surface acoustic wave (SAW) devices, and second-order nonlinear optical materials. Another interesting and important example of the properties can be found in so-called high- $T_c$  superconductors. The copper oxide-based superconductors mainly discovered at the end of 80's such as  $(\text{La,Ba})_2\text{CuO}_4$ ,  $\text{YBa}_2\text{Cu}_3\text{O}_7$ ,  $\text{Bi}_2\text{Ca}_2\text{Sr}_2\text{Cu}_3\text{O}_{10}$ , and so forth have perovskite-related structures.  $\text{SrTiO}_3$  also crystallizes in a perovskite structure and becomes a superconductor when oxygen vacancy is introduced or dopants such as  $\text{La}^{3+}$  and  $\text{Nb}^{5+}$  are incorporated although its critical temperature is rather low;  $T_c=0.1$  to  $0.7$  K depending on the concentration of defect or dopant.<sup>1-4</sup> For  $\text{SrTiO}_3$ , recent study has revealed that two-dimensional electron gas is generated and leads to superconducting transition at 200 mK at an interface between  $\text{SrTiO}_3$  and  $\text{LaAlO}_3$  although both of the oxides are insulators.<sup>5</sup> Also, two-dimensional electron gas confined in Nb-doped  $\text{SrTiO}_3$  quantum well formed in between  $\text{SrTiO}_3$  layers gives rise to a very large thermoelectric Seebeck coefficient.<sup>6</sup> It is well-known that the  $\text{SrTiO}_3$  itself shows quantum paraelectric behavior at low temperatures.

1  
2  
3  
4  
5  
6 As for magnetic properties of oxides with perovskite structure, compounds containing  
7  
8 transition metal ion with mixed valence state, such as (La,Sr)MnO<sub>3</sub> and (La,Sr)CoO<sub>3</sub>, show  
9  
10 ferromagnetism at room temperature owing to the double exchange interaction between  
11  
12 transition metal ions. These oxides are fairly rare examples of ferromagnetic oxides; most of  
13  
14 the oxides are rather antiferromagnetic or ferrimagnetic below their magnetic transition  
15  
16 temperature. Because the ferromagnetism observed in these oxides is closely associated with  
17  
18 the conduction of charged carriers, the oxides, in particular manganese oxide-based compounds,  
19  
20 have arrested a great deal of attention from a point of view of application to spintronics.  
21  
22 Indeed, for the compounds such as (La,Ca)MnO<sub>3</sub>, (La,Sr)MnO<sub>3</sub>, (La,Ba)MnO<sub>3</sub>, and  
23  
24 (Pr,Ca)MnO<sub>3</sub>, giant magnetoresistance (GMR) or colossal magnetoresistance (CMR) has been  
25  
26 observed.<sup>7-12</sup> Furthermore, some of the oxides with perovskite-related structure are regarded as  
27  
28 multiferroics, in which magnetically and dielectrically ordered states such as ferromagnetism  
29  
30 and ferroelectricity coexist because of strong coupling between spin and phonon mode in the  
31  
32 materials.<sup>13,14</sup> For instance, BiMnO<sub>3</sub>, which has a strained perovskite structure, shows  
33  
34 ferromagnetic-paramagnetic phase transition at 105 K and at the same time, manifests  
35  
36 ferroelectric-paraelectric transition at 750 to 770 K.<sup>15</sup> Similar behavior was observed for  
37  
38 BiFeO<sub>3</sub><sup>16</sup> and TbMnO<sub>3</sub>.<sup>17</sup>  
39  
40  
41  
42  
43  
44  
45  
46

47 EuTiO<sub>3</sub> is also an oxide adopting perovskite structure and possessing interesting electrical  
48  
49 and magnetic properties. Similarly to SrTiO<sub>3</sub>, EuTiO<sub>3</sub> as a stable phase crystallizes in a cubic  
50  
51 perovskite structure at room temperature and atmospheric pressure. The lattice constant of  
52  
53 EuTiO<sub>3</sub> is 0.3905 nm at ambient temperature and pressure. This value is just the same as the  
54  
55 lattice constant of SrTiO<sub>3</sub>, as naturally expected from the similarity in ionic radii between Sr<sup>2+</sup>  
56  
57  
58  
59  
60

1  
2  
3  
4  
5  
6 and  $\text{Eu}^{2+}$ . In addition, not only  $\text{SrTiO}_3$  but  $\text{EuTiO}_3$  exhibits quantum paraelectric behavior at  
7  
8 low temperatures. On the other hand, magnetic moment due to  $4f^7$  spins localized at the  $\text{Eu}^{2+}$   
9  
10 site brings about magnetic properties which are peculiar to  $\text{EuTiO}_3$  but are absent in  $\text{SrTiO}_3$ . It  
11  
12 is known that the ensemble of magnetic moments of  $\text{Eu}^{2+}$  ions form a G-type antiferromagnetic  
13  
14 ordering in  $\text{EuTiO}_3$  below 5.3 K.<sup>18,19</sup> Moreover, a strong coupling between spin and soft  
15  
16 phonon mode exists in  $\text{EuTiO}_3$ , as demonstrated by the experimental fact that not only magnetic  
17  
18 susceptibility but dielectric constant manifests a drastic change at the Néel temperature, i.e.,  
19  
20  $T_N=5.3$  K.<sup>20</sup>  $\text{EuZrO}_3$ , which adopts an orthorhombic perovskite structure at room  
21  
22 temperature<sup>21,22</sup> and shows antiferromagnetic transition at 4.1 K,<sup>22</sup> exhibits a similar  
23  
24 magnetodielectric effect. The dielectric constant of  $\text{EuZrO}_3$  is strongly dependent on an  
25  
26 applied magnetic field below the Néel temperature.<sup>23</sup> These phenomena are of interest in  
27  
28 relation to the multiferroics mentioned above.  
29  
30  
31  
32  
33

34  
35 Recently, theoretical approaches have been carried out to dependence of magnetic and  
36  
37 dielectric properties on a strain or a change in lattice volume for  $\text{EuTiO}_3$ , and interesting results  
38  
39 have been derived. Fennie and Rabe<sup>24</sup> predicted that both ferromagnetic and ferroelectric  
40  
41 states are stabilized when a biaxial compressive stress is applied to induce a strain larger than  
42  
43 1.2 % in the plane parallel to the surface of  $\text{EuTiO}_3$  thin film although the stable phase of  
44  
45  $\text{EuTiO}_3$  is antiferromagnetic and quantum paraelectric at low temperatures as described above.  
46  
47 In their calculations, the biaxial compressive strain is introduced in the surface of thin film  
48  
49 while the lattice volume is kept constant, so that the lattice is elongated in a direction  
50  
51 perpendicular to the film surface. Ranjan et al.<sup>25</sup> performed theoretical calculations based on  
52  
53 LDA (local density approximation) + U approach and found that ferromagnetic state becomes  
54  
55  
56  
57  
58  
59  
60

1  
2  
3  
4  
5  
6 more stable than G-type antiferromagnetic state as either the lattice volume of  $\text{EuTiO}_3$  or the  
7  
8 on-site Coulomb repulsion  $U$  for a 4f electron of  $\text{Eu}^{2+}$  ion is increased. Akamatsu et al.<sup>26</sup>  
9  
10 carried out hybrid Hartree-Fock density functional calculations and revealed that as the lattice  
11  
12 volume of  $\text{EuTiO}_3$  is isotropically increased, the exchange coupling constant between  
13  
14 nearest-neighbor  $\text{Eu}^{2+}$  ions increases and changes its sign from negative to positive above a  
15  
16 critical value of lattice volume. This means that the increase in lattice volume leads to the  
17  
18 stabilization of ferromagnetic phase in  $\text{EuTiO}_3$ . The result deduced by Akamatsu et al. is  
19  
20 described below in detail.  
21  
22  
23  
24

25 On the other hand, experimental approaches have been also performed to the relation  
26  
27 between a strain or a lattice volume and magnetic as well as dielectric properties of  $\text{EuTiO}_3$ .  
28  
29 Fujita et al.<sup>27</sup> found that as-deposited  $\text{EuTiO}_3$  thin film on  $\text{SrTiO}_3$  (001) substrate has a lattice  
30  
31 constant elongated by 2.4 % in a direction perpendicular to the film surface and behaves as a  
32  
33 ferromagnet at low temperatures, whereas post-annealed  $\text{EuTiO}_3$  possesses a lattice constant just  
34  
35 the same as those of bulk  $\text{EuTiO}_3$  as well as  $\text{SrTiO}_3$  substrate and shows antiferromagnetic  
36  
37 transition at 5.1 K, as expected for the stable phase of  $\text{EuTiO}_3$ . This fact suggests that the  
38  
39 ferromagnetic behavior is brought about by the increase in lattice volume observed for the  
40  
41 as-deposited  $\text{EuTiO}_3$  thin film, as theoretically predicted for the relation between magnetic  
42  
43 structure and lattice volume of  $\text{EuTiO}_3$ . By following the theoretical calculations performed  
44  
45 by Fennie and Rabe,<sup>24</sup> Lee et al.<sup>28</sup> carried out spin-polarized GGA (generalized gradient  
46  
47 approximation) +  $U$  approach to the  $\text{EuTiO}_3$  thin film, and clarified that tensile as well as  
48  
49 compressive strain gives rise to the stabilization of ferromagnetic and ferroelectric phase of  
50  
51  $\text{EuTiO}_3$ . They also experimentally demonstrated that  $\text{EuTiO}_3$  thin film under tensile strain  
52  
53  
54  
55  
56  
57  
58  
59  
60

1  
2  
3  
4  
5  
6 caused by DyScO<sub>3</sub> substrate becomes a ferroelectric ferromagnet due to the strong spin-lattice  
7  
8 coupling. They observed that the intensity of second-harmonic wave generated in the EuTiO<sub>3</sub>  
9  
10 thin film on DyScO<sub>3</sub> substrate gradually increases with a decrease in temperature below about  
11  
12 250 K. This phenomenon was related to the fact that the ferroelectric state is stabilized below  
13  
14 this temperature.  
15

16  
17  
18 The above-mentioned theoretical and experimental results seem to indicate that there  
19  
20 exists a correlation between the strain or the lattice volume and magnetic structure of EuTiO<sub>3</sub>,  
21  
22 but experimental study on the effect of a systematic variation in lattice volume on the magnetic  
23  
24 properties of EuTiO<sub>3</sub> has not been performed. In the present investigation, we achieve a  
25  
26 systematic variation in lattice volume of EuTiO<sub>3</sub> thin film by changing the type of substrate  
27  
28 compound so that the lattice mismatch between the thin film and the substrate leads to a strain  
29  
30 in the plane parallel to the film surface. For the growth of thin films, a pulsed laser deposition  
31  
32 method is utilized. We demonstrate that magnetization at low temperatures correlates with the  
33  
34 lattice volume of EuTiO<sub>3</sub> thin film; the experimental result qualitatively supports the theoretical  
35  
36 prediction. On the other hand, when a SiO<sub>2</sub> glass plate is used as a substrate and it is kept at  
37  
38 room temperature during the deposition process, amorphous EuTiO<sub>3</sub> thin film is obtained.  
39  
40 Interestingly, the amorphous EuTiO<sub>3</sub> thin film is ferromagnetic at low temperatures and the  
41  
42 Curie temperature of the amorphous phase is comparable to the Néel temperature of the  
43  
44 crystalline EuTiO<sub>3</sub>. Amorphous Eu<sub>2</sub>TiO<sub>4</sub> thin film also exhibits ferromagnetic transition, and  
45  
46 the Curie temperature is higher than that of its crystalline counterpart.<sup>29</sup> These are very rare  
47  
48 phenomena; amorphous oxides exhibiting ferromagnetic transition have been never found thus  
49  
50 far, and the magnetic phase transition temperature is usually lower by one order of magnitude  
51  
52  
53  
54  
55  
56  
57  
58  
59  
60

1  
2  
3  
4  
5  
6 for amorphous oxide than for its crystalline counterpart with the identical composition. In this  
7  
8 paper, we report on these fairly interesting phenomena.  
9

## 10 11 12 13 II. EXPERIMENTAL

### 14 15 Sample preparation

16  
17 A pulsed laser deposition (PLD) method was carried out for the synthesis of crystalline  
18  
19  $\text{EuTiO}_3$  thin films.  $\text{Eu}_2\text{Ti}_2\text{O}_7$ , the structure of which is pyrochlore, was used as a target  
20  
21 material. A sintered body of  $\text{Eu}_2\text{Ti}_2\text{O}_7$  was prepared via conventional solid-state reaction  
22  
23 between  $\text{Eu}_2\text{O}_3$  and  $\text{TiO}_2$ . The  $\text{EuTiO}_3$  thin films were grown on (001) plane of  
24  
25 single-crystalline  $\text{LaAlO}_3$ ,  $\text{SrTiO}_3$ , and  $\text{DyScO}_3$ , having the perovskite structure similarly to  
26  
27  $\text{EuTiO}_3$ , as a substrate, so that the different lattice constant among the substrate compounds  
28  
29 could give rise to the difference in lattice volume among  $\text{EuTiO}_3$  thin films deposited on the  
30  
31 substrates. The lattice constant of  $\text{EuTiO}_3$ ,  $\text{LaAlO}_3$ ,  $\text{SrTiO}_3$ , and  $\text{DyScO}_3$  is 0.3905, 0.3790,  
32  
33 0.3905, and 0.3944 nm, respectively. Hence, considering the lattice mismatch between the  
34  
35  $\text{EuTiO}_3$  thin film and the substrate compounds, shrinkage and elongation of lattice in the plane  
36  
37 parallel to the surface of the  $\text{EuTiO}_3$  thin film were anticipated for  $\text{LaAlO}_3$  and  $\text{DyScO}_3$   
38  
39 substrates, respectively, and neither shrinkage nor elongation was expected for  $\text{SrTiO}_3$  substrate.  
40  
41  
42  
43  
44  
45  
46  
47 The target material was irradiated with a pulsed KrF excimer laser operating at a power of 180  
48  
49 mJ, a wavelength of 248 nm, and a repetition rate of 5 Hz. The substrate was set 2.5 cm apart  
50  
51 from the target and kept at 650°C. The deposition was performed under an oxygen partial  
52  
53 pressure of  $1.0 \times 10^{-5}$  Pa.  
54  
55

56  
57 Amorphous thin films with nominal compositions of  $\text{EuTiO}_3$  and  $\text{Eu}_2\text{TiO}_4$  were also  
58  
59  
60

1  
2  
3  
4  
5  
6 prepared by using the PLD method. Polycrystalline  $\text{EuTiO}_3$  was utilized as a target material  
7  
8 for the amorphous  $\text{EuTiO}_3$  thin film. The target material was synthesized via conventional  
9  
10 solid-state reaction. Reagent-grade  $\text{Eu}_2\text{O}_3$  and  $\text{TiO}_2$  were weighed so that the prescribed  
11  
12 composition was obtained and mixed thoroughly. The mixture was pressed into a pellet, and  
13  
14 the pellet was sintered at  $1400^\circ\text{C}$  for 12 h in air. The resultant material was pulverized, mixed  
15  
16 thoroughly, and pressed into a pellet. The pellet was sintered at  $1200^\circ\text{C}$  for 24 h in a reducing  
17  
18 atmosphere of 95 vol% Ar and 5 vol%  $\text{H}_2$ . The process of pulverizing and sintering in the  
19  
20 reducing atmosphere was repeated four times. The sintered body thus obtained was used as  
21  
22 the target. On the other hand, as for the target material to prepare amorphous  $\text{Eu}_2\text{TiO}_4$ ,  
23  
24 reagent-grade  $\text{Eu}_2\text{O}_3$  was first reduced into EuO by mixing  $\text{Eu}_2\text{O}_3$  powder with slightly excess  
25  
26 amount of graphite powder, making a pellet, and sintering at  $1450^\circ\text{C}$  for 6 h in a graphite  
27  
28 crucible under the reducing atmosphere. A sintered body of EuO thus obtained was pulverized  
29  
30 and mixed thoroughly with  $\text{TiO}_2$  powder to reach the prescribed composition. The mixture  
31  
32 was sintered at  $1500^\circ\text{C}$  for 10 h in a graphite crucible under the reducing atmosphere. The  
33  
34 resultant material was used as a target for the preparation of amorphous  $\text{Eu}_2\text{TiO}_4$  thin film.  
35  
36 The target material was set 2.5 cm away from  $\text{SiO}_2$  glass substrate. The deposition of thin  
37  
38 films was performed by irradiating the target with a KrF excimer laser operating at a  
39  
40 wavelength of 248 nm, a repetition rate of 10 Hz, and a fluence of 2 to  $3 \text{ mJ}/\text{cm}^2$ . The  
41  
42 substrate was kept in a vacuum chamber with a base pressure of  $10^{-6}$  Pa, and was not  
43  
44 intentionally heated.  
45  
46  
47  
48  
49  
50  
51  
52

## 53 54 55 56 57 Measurements 58 59 60

1  
2  
3  
4  
5  
6 Rutherford backscattering spectrometry was carried out using a 2.0 MeV  $\text{He}^{2+}$  to estimate  
7  
8 the composition and thickness of the resultant thin films. Atomic force microscopy (AFM)  
9  
10 was performed to observe the surface morphology of the thin films from a point of view of  
11  
12 atomistic level. X-ray diffraction (XRD) with  $\text{CuK}\alpha$  radiation was utilized to identify  
13  
14 crystalline phases and to evaluate the lattice constant for crystalline  $\text{EuTiO}_3$  thin films deposited  
15  
16 on several kinds of substrate. XRD measurements were also carried out to confirm that no  
17  
18 crystalline phases were present in the amorphous thin films. For the crystalline  $\text{EuTiO}_3$  thin  
19  
20 films, X-ray reciprocal space mappings were obtained by using a four-circle XRD apparatus.  
21  
22 High-resolution transmission electron microscopy (HRTEM), selected area electron diffraction  
23  
24 (SAED), and X-ray absorption spectroscopy were also performed for the amorphous thin films.  
25  
26 The extended X-ray absorption fine structure (EXAFS) spectra were obtained for Eu  $L_3$ -edge to  
27  
28 examine the local structure of Eu ion in the amorphous thin films. Details of the procedure of  
29  
30 measurement and analysis of EXAFS were described elsewhere.<sup>30</sup> Variation of magnetization  
31  
32 with temperature and magnetic field was measured by using a superconducting quantum  
33  
34 interference device (SQUID).  
35  
36  
37  
38  
39  
40  
41  
42  
43

### 44 III. RESULTS AND DISCUSSION

#### 45 Lattice volume expansion-induced ferromagnetism of $\text{EuTiO}_3$ thin film

46  
47  
48  
49 The molar ratio of Eu to Ti, estimated by the Rutherford backscattering, in the thin films  
50  
51 deposited on  $\text{LaAlO}_3$ ,  $\text{SrTiO}_3$ , and  $\text{DyScO}_3$  substrates is shown in Table 1. The experimental  
52  
53 error in the molar ratio was evaluated to be 0.15 to 0.70 %. The molar ratio of Eu to Ti is  
54  
55 almost equal to 1 for all the thin films, indicating that the as-deposited thin films are  
56  
57  
58  
59  
60

1  
2  
3  
4  
5  
6 stoichiometric as far as the molar ratio of cations is concerned. Also, it was demonstrated by  
7  
8 the out-of-plane and in-plane XRD measurements that the thin films are composed of single  
9  
10 phase of  $\text{EuTiO}_3$  (although the XRD patterns are not shown here). The data obtained from the  
11  
12 XRD measurements, i.e., the reciprocal space mappings are discussed below in detail. Figure  
13  
14 1 illustrates the AFM image for the  $\text{EuTiO}_3$  thin films on the different types of substrate. LAO,  
15  
16 STO, and DSO indicated in the figure denote the  $\text{LaAlO}_3$ ,  $\text{SrTiO}_3$ , and  $\text{DyScO}_3$  substrates,  
17  
18 respectively. So-called stepped and terraced structure is observed, suggesting that the surface  
19  
20 of the thin films is atomically flat and smooth.  
21  
22  
23  
24

25 Figure 2 depicts the reciprocal space mappings for  $\text{EuTiO}_3$  thin films deposited on  
26  
27  $\text{LaAlO}_3$ ,  $\text{SrTiO}_3$ , and  $\text{DyScO}_3$  substrates.  $Q_x$  and  $Q_y$  stand for the reciprocal lattice vectors  
28  
29 corresponding to the lattice vector parallel and perpendicular to the film surface, respectively.  
30  
31 Bragg spots ascribed to the thin film and the substrate are observed in each of the reciprocal  
32  
33 space mappings. The small circle shown in each of the illustrations denotes the reciprocal  
34  
35 lattice for bulk  $\text{EuTiO}_3$ . It is possible to evaluate a strain or a change in lattice volume for  
36  
37  $\text{EuTiO}_3$  thin film by comparing the reciprocal lattice of the thin film with that of bulk  $\text{EuTiO}_3$ .  
38  
39 In the case that  $\text{LaAlO}_3$  is used as a substrate,  $Q_y$  of  $\text{EuTiO}_3$  thin film is much smaller than that  
40  
41 of bulk  $\text{EuTiO}_3$ , whereas  $Q_x$  is slightly larger for  $\text{EuTiO}_3$  thin film than for bulk  $\text{EuTiO}_3$ . This  
42  
43 fact indicates that the lattice of the  $\text{EuTiO}_3$  thin film is elongated in a direction perpendicular to  
44  
45 the surface of the thin film and slightly shrinks in a direction parallel to the surface. In this  
46  
47 case, the lattice of  $\text{EuTiO}_3$  thin film is elongated by +1.89 % in a direction perpendicular to the  
48  
49 surface and shrinks by -0.3 % in the plane parallel to the surface, respectively. Therefore, the  
50  
51 change in lattice volume from the bulk  $\text{EuTiO}_3$  is evaluated to be +1.56 %. Similar estimation  
52  
53  
54  
55  
56  
57  
58  
59  
60

1  
2  
3  
4  
5  
6 of variation in lattice constant can be performed for the  $\text{SrTiO}_3$  and  $\text{DyScO}_3$  substrates. The  
7  
8 results are summarized in Table 2, where  $\Delta l_1$  and  $\Delta l_2$  denote the variation in lattice constant in a  
9  
10 direction parallel and perpendicular to the surface of the thin film, respectively, and  $\Delta V$  stands  
11  
12 for the change in lattice volume for the  $\text{EuTiO}_3$  thin films. As expected from the degree of  
13  
14 lattice mismatch, the lattice volume of  $\text{EuTiO}_3$  thin film is the largest for the  $\text{DyScO}_3$  substrate  
15  
16 and the smallest for the  $\text{LaAlO}_3$  substrate. For the  $\text{SrTiO}_3$  substrate, an intermediate value is  
17  
18  
19 obtained.  
20  
21

22  
23 Whereas the in-plane lattice constant of  $\text{EuTiO}_3$  thin film is varied by altering the kind of  
24  
25 substrate compound, the out-of-plane lattice constant of  $\text{EuTiO}_3$  thin film is elongated when  
26  
27 compared to the bulk  $\text{EuTiO}_3$  irrespective of the sort of substrate compound. As a result, the  
28  
29 lattice volume of  $\text{EuTiO}_3$  thin film becomes larger than that of bulk  $\text{EuTiO}_3$  even when  $\text{LaAlO}_3$ ,  
30  
31 whose lattice constant is smaller than that of bulk  $\text{EuTiO}_3$ , is used as a substrate. In general,  
32  
33 when the lattice constant is larger for material of thin film than for substrate material, the  
34  
35 in-plane lattice constant of the thin film becomes shorter, and the out-of-plane lattice constant  
36  
37 becomes longer because of the compressive strain at the interface between the thin film and the  
38  
39 substrate.<sup>28,31</sup> For instance, the out-of-plane lattice constant of  $\text{EuTiO}_3$  thin film deposited on  
40  
41  
42  
43  
44  
45  
46  
47  
48  
49  
50  
51  
52  
53  
54  
55  
56  
57  
58  
59  
60  
61  
62  
63  
64  
65  
66  
67  
68  
69  
70  
71  
72  
73  
74  
75  
76  
77  
78  
79  
80  
81  
82  
83  
84  
85  
86  
87  
88  
89  
90  
91  
92  
93  
94  
95  
96  
97  
98  
99  
100  
101  
102  
103  
104  
105  
106  
107  
108  
109  
110  
111  
112  
113  
114  
115  
116  
117  
118  
119  
120  
121  
122  
123  
124  
125  
126  
127  
128  
129  
130  
131  
132  
133  
134  
135  
136  
137  
138  
139  
140  
141  
142  
143  
144  
145  
146  
147  
148  
149  
150  
151  
152  
153  
154  
155  
156  
157  
158  
159  
160  
161  
162  
163  
164  
165  
166  
167  
168  
169  
170  
171  
172  
173  
174  
175  
176  
177  
178  
179  
180  
181  
182  
183  
184  
185  
186  
187  
188  
189  
190  
191  
192  
193  
194  
195  
196  
197  
198  
199  
200  
201  
202  
203  
204  
205  
206  
207  
208  
209  
210  
211  
212  
213  
214  
215  
216  
217  
218  
219  
220  
221  
222  
223  
224  
225  
226  
227  
228  
229  
230  
231  
232  
233  
234  
235  
236  
237  
238  
239  
240  
241  
242  
243  
244  
245  
246  
247  
248  
249  
250  
251  
252  
253  
254  
255  
256  
257  
258  
259  
260  
261  
262  
263  
264  
265  
266  
267  
268  
269  
270  
271  
272  
273  
274  
275  
276  
277  
278  
279  
280  
281  
282  
283  
284  
285  
286  
287  
288  
289  
290  
291  
292  
293  
294  
295  
296  
297  
298  
299  
300  
301  
302  
303  
304  
305  
306  
307  
308  
309  
310  
311  
312  
313  
314  
315  
316  
317  
318  
319  
320  
321  
322  
323  
324  
325  
326  
327  
328  
329  
330  
331  
332  
333  
334  
335  
336  
337  
338  
339  
340  
341  
342  
343  
344  
345  
346  
347  
348  
349  
350  
351  
352  
353  
354  
355  
356  
357  
358  
359  
360  
361  
362  
363  
364  
365  
366  
367  
368  
369  
370  
371  
372  
373  
374  
375  
376  
377  
378  
379  
380  
381  
382  
383  
384  
385  
386  
387  
388  
389  
390  
391  
392  
393  
394  
395  
396  
397  
398  
399  
400  
401  
402  
403  
404  
405  
406  
407  
408  
409  
410  
411  
412  
413  
414  
415  
416  
417  
418  
419  
420  
421  
422  
423  
424  
425  
426  
427  
428  
429  
430  
431  
432  
433  
434  
435  
436  
437  
438  
439  
440  
441  
442  
443  
444  
445  
446  
447  
448  
449  
450  
451  
452  
453  
454  
455  
456  
457  
458  
459  
460  
461  
462  
463  
464  
465  
466  
467  
468  
469  
470  
471  
472  
473  
474  
475  
476  
477  
478  
479  
480  
481  
482  
483  
484  
485  
486  
487  
488  
489  
490  
491  
492  
493  
494  
495  
496  
497  
498  
499  
500  
501  
502  
503  
504  
505  
506  
507  
508  
509  
510  
511  
512  
513  
514  
515  
516  
517  
518  
519  
520  
521  
522  
523  
524  
525  
526  
527  
528  
529  
530  
531  
532  
533  
534  
535  
536  
537  
538  
539  
540  
541  
542  
543  
544  
545  
546  
547  
548  
549  
550  
551  
552  
553  
554  
555  
556  
557  
558  
559  
560  
561  
562  
563  
564  
565  
566  
567  
568  
569  
570  
571  
572  
573  
574  
575  
576  
577  
578  
579  
580  
581  
582  
583  
584  
585  
586  
587  
588  
589  
590  
591  
592  
593  
594  
595  
596  
597  
598  
599  
600  
601  
602  
603  
604  
605  
606  
607  
608  
609  
610  
611  
612  
613  
614  
615  
616  
617  
618  
619  
620  
621  
622  
623  
624  
625  
626  
627  
628  
629  
630  
631  
632  
633  
634  
635  
636  
637  
638  
639  
640  
641  
642  
643  
644  
645  
646  
647  
648  
649  
650  
651  
652  
653  
654  
655  
656  
657  
658  
659  
660  
661  
662  
663  
664  
665  
666  
667  
668  
669  
670  
671  
672  
673  
674  
675  
676  
677  
678  
679  
680  
681  
682  
683  
684  
685  
686  
687  
688  
689  
690  
691  
692  
693  
694  
695  
696  
697  
698  
699  
700  
701  
702  
703  
704  
705  
706  
707  
708  
709  
710  
711  
712  
713  
714  
715  
716  
717  
718  
719  
720  
721  
722  
723  
724  
725  
726  
727  
728  
729  
730  
731  
732  
733  
734  
735  
736  
737  
738  
739  
740  
741  
742  
743  
744  
745  
746  
747  
748  
749  
750  
751  
752  
753  
754  
755  
756  
757  
758  
759  
760  
761  
762  
763  
764  
765  
766  
767  
768  
769  
770  
771  
772  
773  
774  
775  
776  
777  
778  
779  
780  
781  
782  
783  
784  
785  
786  
787  
788  
789  
790  
791  
792  
793  
794  
795  
796  
797  
798  
799  
800  
801  
802  
803  
804  
805  
806  
807  
808  
809  
810  
811  
812  
813  
814  
815  
816  
817  
818  
819  
820  
821  
822  
823  
824  
825  
826  
827  
828  
829  
830  
831  
832  
833  
834  
835  
836  
837  
838  
839  
840  
841  
842  
843  
844  
845  
846  
847  
848  
849  
850  
851  
852  
853  
854  
855  
856  
857  
858  
859  
860  
861  
862  
863  
864  
865  
866  
867  
868  
869  
870  
871  
872  
873  
874  
875  
876  
877  
878  
879  
880  
881  
882  
883  
884  
885  
886  
887  
888  
889  
890  
891  
892  
893  
894  
895  
896  
897  
898  
899  
900  
901  
902  
903  
904  
905  
906  
907  
908  
909  
910  
911  
912  
913  
914  
915  
916  
917  
918  
919  
920  
921  
922  
923  
924  
925  
926  
927  
928  
929  
930  
931  
932  
933  
934  
935  
936  
937  
938  
939  
940  
941  
942  
943  
944  
945  
946  
947  
948  
949  
950  
951  
952  
953  
954  
955  
956  
957  
958  
959  
960  
961  
962  
963  
964  
965  
966  
967  
968  
969  
970  
971  
972  
973  
974  
975  
976  
977  
978  
979  
980  
981  
982  
983  
984  
985  
986  
987  
988  
989  
990  
991  
992  
993  
994  
995  
996  
997  
998  
999  
1000

1  
2  
3  
4  
5  
6 the large elongation of lattice in a direction perpendicular to the surface of the present  $\text{EuTiO}_3$   
7  
8 thin films is that single atomic layers such as  $\text{EuO}$  and  $\text{TiO}_2$  layers may be inserted into the  
9  
10 perovskite structure during the deposition process to form a compound like the  
11  
12 Ruddlesden-Popper phase. However, this possibility can be ruled out, considering the fact that  
13  
14 post-annealing of as-deposited  $\text{EuTiO}_3$  thin film grown on  $\text{SrTiO}_3$  substrate makes the lattice  
15  
16 constant shrink to be just the same as the lattice constant of bulk  $\text{EuTiO}_3$ .<sup>27</sup> Some  
17  
18 oxygen-related point defects may cause the phenomenon, although experimental evidence is  
19  
20 absent at this moment, and hence, further study is needed to solve the problem.  
21  
22  
23  
24

25  
26 Magnetic properties are shown in Figs. 3 and 4 for the  $\text{EuTiO}_3$  thin films deposited on  
27  
28  $\text{LaAlO}_3$ ,  $\text{SrTiO}_3$ , and  $\text{DyScO}_3$  substrates. Figure 3 depicts the temperature dependence of  
29  
30 magnetization measured at an applied magnetic field of 100 Oe for  $\text{EuTiO}_3$  thin films grown on  
31  
32  $\text{LaAlO}_3$  (denoted by diamond),  $\text{SrTiO}_3$  (circle), and  $\text{DyScO}_3$  (square) substrates as well as for  
33  
34 bulk  $\text{EuTiO}_3$  (triangle). The inset of the figure is a magnified view of the magnetization data  
35  
36 for bulk  $\text{EuTiO}_3$ . It is seen that the bulk  $\text{EuTiO}_3$  manifests an antiferromagnetic transition at  
37  
38 about 5 K, as reported in literature.<sup>18,19</sup> In contrast, different behavior is observed for the  
39  
40  $\text{EuTiO}_3$  thin films; the magnetization drastically increases below about 5 K as the temperature is  
41  
42 decreased for all the  $\text{EuTiO}_3$  thin films. Figure 4 illustrates the variation of magnetization with  
43  
44 magnetic field at 2 K for  $\text{EuTiO}_3$  thin films grown on  $\text{LaAlO}_3$  (denoted by diamond),  $\text{SrTiO}_3$   
45  
46 (circle), and  $\text{DyScO}_3$  (square) substrates as well as for bulk  $\text{EuTiO}_3$  (triangle). The insets show  
47  
48 the magnetization at low magnetic fields for  $\text{EuTiO}_3$  thin film grown on  $\text{SrTiO}_3$  substrate (right  
49  
50 inset: circle) and for bulk  $\text{EuTiO}_3$  (left inset: triangle). It is obvious that the magnetic field  
51  
52 dependence of magnetization is different between the  $\text{EuTiO}_3$  thin film and the bulk  $\text{EuTiO}_3$ ; the  
53  
54  
55  
56  
57  
58  
59  
60

1  
2  
3  
4  
5  
6  
7  
8  
9  
10  
11  
12  
13  
14  
15  
16  
17  
18  
19  
20  
21  
22  
23  
24  
25  
26  
27  
28  
29  
30  
31  
32  
33  
34  
35  
36  
37  
38  
39  
40  
41  
42  
43  
44  
45  
46  
47  
48  
49  
50  
51  
52  
53  
54  
55  
56  
57  
58  
59  
60

EuTiO<sub>3</sub> thin film grown on SrTiO<sub>3</sub> substrate manifests magnetic field dependence of magnetization peculiar to a ferromagnet, whereas a spin-flip transition characteristic of an antiferromagnet is clearly observed for the bulk EuTiO<sub>3</sub>. The ferromagnetic behavior is seen for the EuTiO<sub>3</sub> thin films grown on LaAlO<sub>3</sub> and DyScO<sub>3</sub> substrates as well. The results are in good agreement with the temperature dependence of magnetization illustrated in Fig. 3. It is also found in Fig. 4 that the saturation magnetization for the EuTiO<sub>3</sub> thin films is  $6.4\mu_B$  to  $6.8\mu_B$ , where  $\mu_B$  is the Bohr magneton. These values are almost identical to the theoretical magnetic moment of Eu<sup>2+</sup>, i.e.,  $7\mu_B$ , suggesting that almost all the europium ions are present as a divalent state in the thin films. The fact that the valence state of almost all the europium ions in the thin films is +2 was confirmed by conversion electron <sup>151</sup>Eu Mössbauer spectroscopy.<sup>27</sup> For instance, the fraction of Eu<sup>2+</sup> in the total number of europium ion is 96 and 98 % for as-deposited and annealed EuTiO<sub>3</sub> thin films grown on SrTiO<sub>3</sub> substrate, respectively. The fraction of Eu<sup>2+</sup> and Eu<sup>3+</sup> in EuTiO<sub>3</sub>, or strictly speaking, the composition of which is EuTiO<sub>3- $\delta$</sub> , is very important because it may affect the magnetic properties. An increase in the fraction of Eu<sup>3+</sup> possibly raises the concentration of conduction electron, leading to the ferromagnetic order of Eu<sup>2+</sup> ions through the mechanism of magnetic polaron or Ruderman-Kittel-Kasuya-Yoshida (RKKY) interaction. The fact that the fraction of Eu<sup>3+</sup> is fairly small in the preset EuTiO<sub>3</sub> thin films rules out the possibility of these mechanisms for the ferromagnetism observed in the present thin films. This is further supported by the fact that the evident antiferromagnetic transition occurs in the annealed EuTiO<sub>3</sub> thin film whereas the ferromagnetism is observed in the as-deposited EuTiO<sub>3</sub> thin film although the fraction of Eu<sup>3+</sup> in the annealed EuTiO<sub>3</sub> thin film is almost the same as that in the as-deposited EuTiO<sub>3</sub> thin film.<sup>27</sup>

1  
2  
3  
4  
5  
6 A look at magnetization shown in Fig. 3 reveals that the low-temperature magnetization is  
7  
8 the highest for DyScO<sub>3</sub> substrate, intermediate for SrTiO<sub>3</sub>, and the lowest for LaAlO<sub>3</sub> substrate.  
9  
10 Considering the above-mentioned experimental fact that the lattice volume of EuTiO<sub>3</sub> thin film  
11  
12 depends on the sort of substrate compound and increases in the order that DyScO<sub>3</sub> > SrTiO<sub>3</sub> >  
13  
14 LaAlO<sub>3</sub>, it seems that the low-temperature magnetization monotonically increases with an  
15  
16 increase in the lattice volume of EuTiO<sub>3</sub> thin film. This tendency is coincident with the result  
17  
18 derived by theoretical approaches.<sup>25,26</sup> Akamatsu et al.<sup>26</sup> calculated energy for different spin  
19  
20 configurations in EuTiO<sub>3</sub> as shown in Fig. 5 by using the hybrid Hartree-Fock density  
21  
22 functional approach. When a prototype of spin-Hamiltonian for Heisenberg system  
23  
24  
25

$$26 \quad H_{\text{spin}} = -2 \sum_{i>j} J_{ij} \mathbf{S}_i \cdot \mathbf{S}_j \quad (1)$$

27  
28 is assumed, the energy of spin system is expressed by

$$29 \quad E_F = E_0 + 2S(S+1)(-12J_1 - 24J_2), \quad (2)$$

30  
31 and

$$32 \quad E_G = E_0 + 2S(S+1)(12J_1 - 24J_2), \quad (3)$$

33  
34 for ferromagnetic and G-type antiferromagnetic spin configurations in EuTiO<sub>3</sub> lattice,  
35  
36 respectively. Here, J<sub>1</sub> and J<sub>2</sub> stand for the exchange coupling constant for the  
37  
38 nearest-neighboring and the next-nearest-neighboring Eu<sup>2+</sup> ions, respectively (see Fig. 5).  
39  
40 Equations (2) and (3) indicate that the difference in energy between ferromagnetic and G-type  
41  
42 antiferromagnetic states depends only on the sign of J<sub>1</sub>. In other words, whether the  
43  
44 ferromagnetic or G-type antiferromagnetic state is stable for 4f spins in EuTiO<sub>3</sub> is determined  
45  
46 only by the exchange interaction among the nearest-neighboring Eu<sup>2+</sup> ions. The hybrid  
47  
48  
49  
50  
51  
52  
53  
54  
55  
56  
57  
58  
59  
60

1  
2  
3  
4  
5  
6 Hartree-Fock density functional approach indicates that the exchange coupling constant  $J_1$   
7  
8 monotonically increases as the lattice volume of  $\text{EuTiO}_3$  increases and that  $J_1$  changes its sign  
9  
10 from negative to positive when an increase in lattice volume of  $\text{EuTiO}_3$  exceeds about 5 %.<sup>26</sup>  
11  
12 Subsequently, the ferromagnetic state becomes more stable than the G-type antiferromagnetic  
13  
14 state when the lattice volume is increased beyond this critical value. The result derived from  
15  
16 the calculations that  $J_1$  is positive and monotonically increases with an increase in the lattice  
17  
18 volume above the critical value is qualitatively coincident with the present experimental result  
19  
20 shown in Fig. 3 and Table 2.  
21  
22  
23

24  
25 The calculations by Akamatsu et al. also suggest that the overlap between the 4f orbital of  
26  
27  $\text{Eu}^{2+}$  and the 3d orbital of  $\text{Ti}^{4+}$  in the  $\text{EuTiO}_3$  lattice becomes more significant as the lattice  
28  
29 volume is decreased.<sup>26</sup> It should be noted that an overlap between the Eu 4f and the O 2p  
30  
31 orbitals does not take place even when the lattice volume is decreased. The overlap between  
32  
33 the 4f orbital of  $\text{Eu}^{2+}$  and the 3d orbital of  $\text{Ti}^{4+}$  can bring about the superexchange interaction  
34  
35 between the nearest-neighboring  $\text{Eu}^{2+}$  ions, leading to antiferromagnetic configuration of  
36  
37 magnetic moments of  $\text{Eu}^{2+}$  ions. This idea stems from the fact that the Eu 4f orbital is  
38  
39 non-orthogonal to the Ti 3d orbital. According to Anderson's theory of superexchange  
40  
41 interaction,<sup>32</sup> antiferromagnetic coupling is stabilized by the overlap between magnetic orbitals  
42  
43 through intervening orbital, such as p state of non-magnetic anion, which is non-orthogonal to  
44  
45 the magnetic orbital. Hence, the superexchange interaction between  $\text{Eu}^{2+}$  ions via the Ti 3d  
46  
47 states is expected to be antiferromagnetic. On the other hand, the indirect exchange coupling  
48  
49 between 4f spins via 5d state of  $\text{Eu}^{2+}$  gives rise to ferromagnetic interaction between the  
50  
51 nearest-neighboring  $\text{Eu}^{2+}$  ions.<sup>19,33-35</sup> The mechanism to bring about the ferromagnetic  
52  
53  
54  
55  
56  
57  
58  
59  
60

1  
2  
3  
4  
5  
6 interaction is schematically illustrated in Fig. 6. The indirect exchange interaction is such a  
7  
8 process that an electron excited from the 4f level into the vacant 5d level of an  $\text{Eu}^{2+}$  ion is  
9  
10 transferred to the 5d level of the nearest-neighbor  $\text{Eu}^{2+}$  ion and interacts with 4f spins at the  
11  
12  $\text{Eu}^{2+}$  ion so that the spins in 5d and 4f states are parallel. These antiferromagnetic and  
13  
14 ferromagnetic interactions compete with each other. The superexchange interaction via 3d  
15  
16 state of  $\text{Ti}^{4+}$  becomes weaker as the lattice volume of  $\text{EuTiO}_3$  is increased, because of the less  
17  
18 overlapping between 4f orbital of  $\text{Eu}^{2+}$  and 3d orbital of  $\text{Ti}^{4+}$ . At the same time, the indirect  
19  
20 exchange coupling between 4f spins via 5d state of  $\text{Eu}^{2+}$  to bring about ferromagnetic  
21  
22 configuration becomes weaker as the lattice volume of  $\text{EuTiO}_3$  is increased, because the  
23  
24 separation between the nearest-neighbor  $\text{Eu}^{2+}$  ions becomes longer as the lattice volume is  
25  
26 increased.<sup>34,35</sup> In  $\text{EuTiO}_3$ , the superexchange interaction via  $\text{Ti}^{4+}$  3d state becomes less  
27  
28 dominant than the indirect exchange coupling via  $\text{Eu}^{2+}$  5d state as the lattice volume becomes  
29  
30 larger. Consequently, ferromagnetic phase is stabilized in  $\text{EuTiO}_3$  with expanded lattice  
31  
32 volume.  
33  
34  
35  
36  
37  
38  
39  
40  
41

#### 42 Ferromagnetism of amorphous $\text{EuTiO}_3$ and $\text{Eu}_2\text{TiO}_4$ thin films

43  
44 An attempt was made to synthesize amorphous  $\text{EuTiO}_3$  and  $\text{Eu}_2\text{TiO}_4$  thin films on  $\text{SiO}_2$   
45  
46 glass substrate by using the PLD method. According to the RBS measurements, the molar  
47  
48 ratio of Eu to Ti is estimated to be 1.00:1.00 and 2.00:1.06 for thin films prepared from the  
49  
50 target materials with  $\text{EuTiO}_3$  and  $\text{Eu}_2\text{TiO}_4$  compositions, respectively; the molar ratio for the  
51  
52 thin films is almost identical to that for the target materials. Figure 7 shows the XRD patterns  
53  
54 for  $\text{EuTiO}_3$  and  $\text{Eu}_2\text{TiO}_4$  thin films as well as HRTEM image and SAED pattern for  $\text{EuTiO}_3$ .  
55  
56  
57  
58  
59  
60

1  
2  
3  
4  
5  
6 In the figure, a-ETO and a-2ETO stand for the thin films with  $\text{EuTiO}_3$  and  $\text{Eu}_2\text{TiO}_4$   
7  
8 compositions, respectively. No sharp diffraction lines ascribable to crystalline phases but halo  
9  
10 patterns peculiar to amorphous structure are observed in the XRD diagrams, suggesting that the  
11  
12 thin films are amorphous and include no crystalline phases. The halo patterns at around  $2\theta =$   
13  
14  $30^\circ$  and  $20^\circ$  are attributable to the thin film and  $\text{SiO}_2$  glass substrate, respectively. The  
15  
16 HRTEM image and the SAED pattern also indicate that the  $\text{EuTiO}_3$  thin film contains no  
17  
18 crystalline phases, confirming that the thin film is amorphous. Similar results were derived for  
19  
20 the  $\text{Eu}_2\text{TiO}_4$  thin film from its HRTEM image and SAED pattern.  
21  
22  
23  
24

25  
26 Figure 8 illustrates the variation of magnetization with temperature measured at an  
27  
28 applied dc magnetic field of 100 Oe for the amorphous  $\text{EuTiO}_3$  and  $\text{Eu}_2\text{TiO}_4$  thin films. The  
29  
30 magnetization is very low at high temperatures; the temperature dependence of magnetic  
31  
32 susceptibility at high temperatures is describable in terms of the Curie-Weiss law:  
33

$$\chi = \frac{NM_B^2 \mu_B^2}{3k_B(T - \theta_w)} \quad (4)$$

34  
35  
36  
37  
38 where  $\chi$  is the magnetic susceptibility, T is the temperature, N is the number density of magnetic  
39  
40 moment,  $\mu_B$  is the Bohr magneton,  $M_B$  is the effective number of Bohr magnetons,  $k_B$  is the  
41  
42 Boltzmann constant, and  $\theta_w$  is the Weiss temperature. On the other hand, as the temperature is  
43  
44 decreased, the magnetization increases drastically below a certain temperature. The behavior  
45  
46 indicates that the thin films are ferromagnetic at low temperatures. The Curie temperature  
47  
48 estimated as an inflection point (as indicated by an arrow in Fig. 8) in the magnetization as a  
49  
50 function of temperature is  $T_C = 5.5$  K and 14 K for the amorphous  $\text{EuTiO}_3$  and  $\text{Eu}_2\text{TiO}_4$ ,  
51  
52  
53 respectively. First of all, it is surprising that amorphous  $\text{EuTiO}_3$  exhibits ferromagnetic phase  
54  
55  
56  
57  
58  
59  
60

1  
2  
3  
4  
5  
6 transition although the stable phase of crystalline  $\text{EuTiO}_3$  is a G-type antiferromagnet as  
7  
8 mentioned above. Besides, the Curie temperature, i.e., 5.5 K is comparable to the Néel  
9  
10 temperature of the crystalline counterpart, i.e., 5.3 K. Secondly, the ferromagnetic phase  
11  
12 transition is observed for the amorphous  $\text{Eu}_2\text{TiO}_4$  thin film as well as crystalline phase of  
13  
14  $\text{Eu}_2\text{TiO}_4$ , and moreover, the Curie temperature of the amorphous phase, i.e.,  $T_C=14$  K is rather  
15  
16 higher than that of crystalline counterpart, i.e.,  $T_C=9$  K.<sup>36</sup> The Weiss temperature derived from  
17  
18 the fit of Eq. (4) to the magnetic susceptibility data at high temperatures is  $\theta_W=+8.0$  and  $+17.6$   
19  
20 K for the amorphous  $\text{EuTiO}_3$  and  $\text{Eu}_2\text{TiO}_4$ , respectively.<sup>29</sup> These values are significantly  
21  
22 higher than the Weiss temperature of their crystalline counterparts, i.e.,  $\theta_W=+3.8$  K<sup>19</sup> and  $+10$   
23  
24 K<sup>35</sup> for crystalline  $\text{EuTiO}_3$  and  $\text{Eu}_2\text{TiO}_4$ , respectively, clearly indicating that the amorphization  
25  
26 enhances the ferromagnetic interaction among  $\text{Eu}^{2+}$  ions. Considering the effect of  
27  
28 amorphization on the magnetic properties for other transition metal oxides, these phenomena are  
29  
30 very rare. In most of the amorphous oxides or oxide glasses containing 3d transition metal  
31  
32 and/or trivalent rare-earth ions, antiferromagnetic rather than ferromagnetic interaction is  
33  
34 predominant among the magnetic ions.<sup>37-46</sup> Furthermore, it is usual that the magnetic transition  
35  
36 temperature is decreased by one order of magnitude when crystalline oxides are made to be  
37  
38 amorphous with the composition kept constant. For instance, whereas crystalline  $\alpha\text{-Fe}_2\text{O}_3$  is  
39  
40 known to show weak ferromagnetism below 950 K, amorphous  $\text{Fe}_2\text{O}_3$  manifests a cluster spin  
41  
42 glass transition at  $35.1\pm 0.1$  K.<sup>40</sup> Also, amorphous  $\text{BiFeO}_3$  shows a spin glass transition at 20  
43  
44 K<sup>39</sup> while crystalline  $\text{BiFeO}_3$  is antiferromagnetic with Néel temperature of 643 K.<sup>47</sup> The  
45  
46 ferromagnetic interaction observed even in an amorphous oxide is characteristic of the  $\text{Eu}^{2+}$  ion,  
47  
48 as positive Weiss temperature was observed for some oxide glasses containing a large amount  
49  
50  
51  
52  
53  
54  
55  
56  
57  
58  
59  
60

1  
2  
3  
4  
5  
6 of  $\text{Eu}^{2+}$  ions.<sup>48,49</sup> The ferromagnetic phase transition was also observed for aluminoborosilicate  
7  
8 glass containing 60.0 mol% of  $\text{EuO}$ , although the Curie temperature is as low as 2.2 K.<sup>49</sup>  
9

10  
11 Figure 9 depicts the magnetic field dependence of magnetization measured at 2.0 K for  
12  
13 the amorphous  $\text{EuTiO}_3$  and  $\text{Eu}_2\text{TiO}_4$  thin films. In this figure, the theoretical magnetization  
14  
15 curve calculated by using the Brillouin function for paramagnetic  $\text{Eu}^{2+}$  ion at 2.0 K is also  
16  
17 shown. The slope of the magnetization curve at low magnetic fields is steeper for the  
18  
19 amorphous  $\text{EuTiO}_3$  and  $\text{Eu}_2\text{TiO}_4$  than for the Brillouin function. This fact suggests that the  
20  
21 ferromagnetic interaction is dominant in the amorphous thin films. We can estimate the  
22  
23 magnetic moment per Eu ion to be  $7\mu_B$  from the saturation magnetization at high magnetic  
24  
25 fields for both of the thin films. This value is coincident with the theoretical one for  $4f^7$  state  
26  
27 of  $\text{Eu}^{2+}$ , indicating that almost all the europium ions are present as a divalent state in the  
28  
29 amorphous thin films.  
30  
31  
32  
33

34  
35 The reason why the ferromagnetic state is stabilized in the amorphous  $\text{EuTiO}_3$  and  
36  
37  $\text{Eu}_2\text{TiO}_4$  thin films can be understood in terms of the local structure of  $\text{Eu}^{2+}$  in the amorphous  
38  
39 phases and the above-mentioned mechanism to bring about the ferromagnetic interaction among  
40  
41  $\text{Eu}^{2+}$  ions. Figures 10 (a) and (b) illustrate experimental EXAFS spectra (EXAFS oscillation  
42  
43 curves  $\chi(R)$ s as a function of radial distance) at Eu  $L_3$ -edge (denoted by open squares) for the  
44  
45 amorphous  $\text{EuTiO}_3$  and  $\text{Eu}_2\text{TiO}_4$  thin films, respectively. The insets depict the EXAFS  
46  
47 oscillation curves in the  $q$ -space. The solid curves stand for the best-fits of theoretical ones to  
48  
49 the first Eu–O coordination peaks. Structural parameters evaluated from the analysis, i.e., the  
50  
51 average coordination number of  $\text{Eu}^{2+}$ ,  $n_{\text{Eu}^{2+}}$ , and the nearest Eu–O bond length,  $d_{\text{Eu-O}}$ , are listed  
52  
53 in Table 3. For crystalline  $\text{EuTiO}_3$ ,  $n_{\text{Eu}^{2+}}=12$  and  $d_{\text{Eu-O}}=0.275$  nm, and for crystalline  $\text{Eu}_2\text{TiO}_4$ ,  
54  
55  
56  
57  
58  
59  
60

1  
2  
3  
4  
5  
6 the structure of which is  $K_2NiF_4$ -type,  $n_{Eu^{2+}}=9$  and  $d_{Eu-O}=0.270$  nm (an averaged value).<sup>19</sup>  
7  
8 Hence, both the coordination number of  $Eu^{2+}$  and the Eu-O bond length are much smaller for  
9  
10 the amorphous  $EuTiO_3$  and  $Eu_2TiO_4$  than for their crystalline counterparts. The coordination  
11  
12 number and the Eu-O bond strength in the amorphous phases are rather similar to those of  
13  
14 crystalline EuO with rock salt-type structure, for which  $n_{Eu^{2+}}=6$  and  $d_{Eu-O}=0.257$  nm.<sup>18</sup> The  
15  
16 result of the structural analysis on the EXAFS spectra discloses the origin of the ferromagnetic  
17  
18 interaction stronger in the amorphous thin films than in their crystalline counterparts. The  
19  
20 indirect exchange interaction illustrated in Fig.6 is proportional to  $J_{intra}b^2/U_{fd}^2$ , where  $J_{intra}$  is the  
21  
22 intra-atomic exchange coupling constant between the 4f and 5d levels of  $Eu^{2+}$ ,  $b$  is the transfer  
23  
24 integral between the nearest-neighboring  $Eu^{2+}$  ions, and  $U_{fd}$  is the difference in energy between  
25  
26 the 4f and 5d levels. As readily seen from Fig. 6,  $U_{fd}$  becomes smaller as the crystal field  
27  
28 splitting of 5d level is greater, leading to stronger ferromagnetic interactions.<sup>19</sup> For instance,  
29  
30 the crystal field is much stronger in crystalline EuO than in crystalline  $EuTiO_3$  because the  
31  
32 coordination number of  $Eu^{2+}$  is 6 in the former and 12 in the latter. Subsequently, the  
33  
34 ferromagnetic interaction among  $Eu^{2+}$  ions is so strong that Curie temperature as high as 77 K is  
35  
36 observed in crystalline  $EuO$ ,<sup>50</sup> while antiferromagnetic transition takes place at rather low  
37  
38 temperature like 5.3 K in crystalline  $EuTiO_3$ . Since the coordination number of  $Eu^{2+}$  and Eu-O  
39  
40 bond length in the amorphous  $EuTiO_3$  and  $Eu_2TiO_4$  are rather close to those in crystalline EuO  
41  
42 as demonstrated by the EXAFS spectra, the crystal field splitting of 5d level is larger in the  
43  
44 amorphous  $EuTiO_3$  and  $Eu_2TiO_4$  than in their crystalline counterparts, resulting in the  
45  
46 enhancement of ferromagnetic interaction in the amorphous phases.  
47  
48  
49  
50  
51  
52  
53  
54

55  
56 The stabilization of ferromagnetic state by the amorphization was also observed in  
57  
58  
59  
60

1  
2  
3  
4  
5  
6  
7  
8  
9  
10  
11  
12  
13  
14  
15  
16  
17  
18  
19  
20  
21  
22  
23  
24  
25  
26  
27  
28  
29  
30  
31  
32  
33  
34  
35  
36  
37  
38  
39  
40  
41  
42  
43  
44  
45  
46  
47  
48  
49  
50  
51  
52  
53  
54  
55  
56  
57  
58  
59  
60

EuZrO<sub>3</sub>.<sup>51</sup> Crystalline EuZrO<sub>3</sub> is an antiferromagnet with the Néel temperature of 4.1K,<sup>22</sup> whereas amorphous EuZrO<sub>3</sub> thin film prepared by the PLD method shows ferromagnetic transition at 8 K.<sup>51</sup> It should be noted that the magnetic transition temperature is higher for the amorphous phase than for its crystalline counterpart. The mechanism based on the indirect exchange interaction leads to the ferromagnetic configuration of magnetic moments of Eu<sup>2+</sup> ions in the amorphous EuZrO<sub>3</sub> similarly to the amorphous EuTiO<sub>3</sub> and Eu<sub>2</sub>TiO<sub>4</sub>.

#### IV. CONCLUSIONS

We have synthesized single-crystalline EuTiO<sub>3</sub> thin films on different kinds of substrate, i.e., LaAlO<sub>3</sub>, SrTiO<sub>3</sub>, and DyScO<sub>3</sub> by using a PLD method so that the strain induced at the interface between the thin film and the substrate due to lattice mismatch leads to a change in lattice volume of the EuTiO<sub>3</sub> thin film, and examined the effect of strain on magnetic properties of the resultant EuTiO<sub>3</sub> thin films. All the as-deposited EuTiO<sub>3</sub> thin films manifest elongation of lattice by about 2 % in a direction perpendicular to the surface of the thin films, whereas the in-plane lattice constant of the thin films is determined by the lattice mismatch, so that the contraction and elongation of the lattice in a direction parallel to the surface of the EuTiO<sub>3</sub> thin film are observed for LaAlO<sub>3</sub> and DyScO<sub>3</sub> substrates, respectively. Subsequently, the lattice volume of the EuTiO<sub>3</sub> thin film increases in the order that DyScO<sub>3</sub> > SrTiO<sub>3</sub> > LaAlO<sub>3</sub>. The temperature and magnetic field dependence of magnetization indicates that all the EuTiO<sub>3</sub> thin films exhibit ferromagnetic transition at low temperatures. Besides, the magnetization at low temperatures monotonically increases in the order that DyScO<sub>3</sub> > SrTiO<sub>3</sub> > LaAlO<sub>3</sub>; namely, the magnetization at low temperatures increases with an increase in lattice volume for the

1  
2  
3  
4  
5  
6 as-deposited  $\text{EuTiO}_3$  thin film. The result is qualitatively coincident with the calculations  
7  
8 based on hybrid Hartree-Fock density functional approach that the exchange coupling constant  
9  
10  $J_1$  increases and changes its sign from negative to positive as the lattice volume of  $\text{EuTiO}_3$  is  
11  
12 increased. The amorphous phase of  $\text{EuTiO}_3$  and  $\text{Eu}_2\text{TiO}_4$  synthesized by the PLD method as a  
13  
14 thin film form on  $\text{SiO}_2$  substrate is also ferromagnetic when the temperature is decreased. It is  
15  
16 interesting that amorphous  $\text{EuTiO}_3$  is ferromagnetic although the crystalline counterpart is  
17  
18 antiferromagnetic; it is a very rare case that amorphization makes an antiferromagnetic  
19  
20 compound ferromagnetic. Furthermore, the magnetic transition temperature of amorphous  
21  
22 phase is compared to or higher than that of the crystalline counterpart for  $\text{EuTiO}_3$  and  $\text{Eu}_2\text{TiO}_4$ ,  
23  
24 respectively. The larger ferromagnetic interaction in the amorphous phases can be explained in  
25  
26 terms of the local structure of  $\text{Eu}^{2+}$  similar to the chemical environment around  $\text{Eu}^{2+}$  in  
27  
28 ferromagnetic crystal  $\text{EuO}$ . It is concluded that the indirect exchange interaction via 5d state  
29  
30 of  $\text{Eu}^{2+}$  overcomes the superexchange interaction via  $\text{Ti}^{4+}$  3d state in the magnetic interaction  
31  
32 among the  $\text{Eu}^{2+}$  ions, leading to not only the strain-induced ferromagnetism observed for  
33  
34  $\text{EuTiO}_3$  but also the ferromagnetism caused by amorphization for  $\text{EuTiO}_3$  and  $\text{Eu}_2\text{TiO}_4$ .  
35  
36  
37  
38  
39  
40  
41  
42  
43  
44  
45  
46  
47  
48  
49  
50  
51  
52  
53  
54  
55  
56  
57  
58  
59  
60

## REFERENCES

1. J. F. Schooley, W. R. Hosler, E. Ambler, J. H. Becker, M. L. Cohen, and C. S. Koonce: Dependence of the superconducting transition temperature on carrier concentration in semiconducting SrTiO<sub>3</sub>. *Phys. Rev. Lett.* 14, 305 (1965).
2. A. Baratoff and G. Binnig: Mechanism of superconductivity in SrTiO<sub>3</sub>. *Physica B* 108, 1335 (1981).
3. A. Leitner, C. T. Rogers, J. C. Price, D. A. Rudman, and D. R. Herman: Pulsed laser deposition of superconducting Nb-doped strontium titanate thin films. *Appl. Phys. Lett.* 72, 3065 (1998).
4. D. Olaya, F. Pan, C. T. Rogers, and J. C. Price: Superconductivity in La-doped strontium titanate thin films. *Appl. Phys. Lett.* 84, 4020 (2004).
5. N. Reyren, S. Thiel, A. D. Caviglia, L. Fitting Kourkoutis, G. Hammerl, C. Richter, C. W. Schneider, T. Kopp, A.-S. Rüetschi, D. Jaccard, M. Gabay, D. A. Muller, J.-M. Triscone, J. Mannhart: Superconducting interfaces between insulating oxides. *Science* 317, 1196 (2007).
6. H. Ohta, S. Kim, Y. Mune, T. Mizoguchi, K. Nomura, S. Ohta, T. Nomura, Y. Nakanishi, Y. Ikuhara, M. Hirano, H. Hosono, and K. Koumoto: Giant thermoelectric Seebeck coefficient of a two-dimensional electron gas in SrTiO<sub>3</sub>. *Nature Mater.* 6, 129 (2007).
7. S. Jin, T. H. Tiefel, M. McCormack, R. A. Fastnacht, R. Ramesh, and L. H. Chen: Thousandfold change in resistivity in magnetoresistive La-Ca-Mn-O films. *Science* 264, 413 (1994).
8. K. Chahara, T. Ohno, M. Kasai, and Y. Kozono: Magnetoresistance in magnetic manganese oxide with intrinsic antiferromagnetic spin structure. *Appl. Phys. Lett.* 63, 1990 (1993).

- 1  
2  
3  
4  
5  
6 9. Y. Tokura, A. Urushibara, Y. Moritomo, T. Arima, A. Asamitsu, G. Kido, and N. Furukawa:  
7  
8 Giant magnetotransport phenomena in filling-controlled Kondo lattice system:  
9  
10  $\text{La}_{1-x}\text{Sr}_x\text{MnO}_3$ . J. Phys. Soc. Jpn. 63, 3931 (1994).  
11  
12  
13 10. A. Urushibara, Y. Moritomo, T. Arima, A. Asamitsu, G. Kido, and Y. Tokura:  
14  
15 Insulator-metal transition and giant magnetoresistance in  $\text{La}_{1-x}\text{Sr}_x\text{MnO}_3$ . Phys. Rev. B 51,  
16  
17 14103 (1995).  
18  
19  
20 11. R. von Helmolt, Meeker, B. Holzapfel, L. Schultz, and K. Samwer: Giant negative  
21  
22 magnetoresistance in perovskitelike  $\text{La}_{2/3}\text{Ba}_{1/3}\text{MnO}_x$  ferromagnetic films. Phys. Rev. Lett. 71,  
23  
24 2331 (1993).  
25  
26  
27 12. Y. Tomioka, A. Asamitsu, Y. Moritomo, and Y. Tokura: Anomalous magnetotransport  
28  
29 properties of  $\text{Pr}_{1-x}\text{Ca}_x\text{MnO}_3$ . J. Phys. Soc. Jpn. 64, 3626 (1995).  
30  
31  
32 13. S. W. Cheong and M. Mostovoy: Multiferroics: a magnetic twist for ferroelectricity. Nature  
33  
34 Mater. 6, 13 (2007).  
35  
36  
37 14. Y. Tokura: Multiferroics as quantum electromagnets. Science 312, 1481 (2006).  
38  
39  
40 15. T. Kimura, S. Kawamoto, I. Yamada, M. Azuma, M. Takano, and Y. Tokura:  
41  
42 Magnetocapacitance effect in multiferroic  $\text{BiMnO}_3$ . Phys. Rev. B 67, 180401 (2003).  
43  
44  
45 16. J. Wang, J. B. Neaton, H. Zheng, V. Nagarajan, S. B. Ogale, B. Liu, D. Viehland, V.  
46  
47 Vaithyanathan, D. G. Schlom, U. V. Waghmare, N. A. Spaldin, K. M. Rabe, M. Wuttig, and  
48  
49 R. Ramesh: Epitaxial  $\text{BiFeO}_3$  multiferroic thin film heterostructures. Science 299, 1719  
50  
51 (2003).  
52  
53  
54 17. T. Kimura, T. Goto, H. Shintani, K. Ishizaka, T. Arima, and Y. Tokura: Magnetic control of  
55  
56 ferroelectric polarization. Nature 426, 55 (2003).  
57  
58  
59  
60

- 1  
2  
3  
4  
5  
6 18. T. R. McGuire, M. W. Shafer, R. J. Joenk, H. A. Alperin, and S. J. Pickart: Magnetic  
7  
8 Structure of  $\text{EuTiO}_3$ . *J. Appl. Phys.* 37, 981 (1966).  
9  
10 19. C.-L. Chien, S. DeBenedetti, and F. De S. Barros: Magnetic properties of  $\text{EuTiO}_3$ ,  $\text{Eu}_2\text{TiO}_4$ ,  
11  
12 and  $\text{Eu}_3\text{Ti}_2\text{O}_7$ . *Phys. Rev. B* 10, 3913 (1974).  
13  
14 20. T. Katsufuji and H. Takagi: Coupling between magnetism and dielectric properties in  
15  
16 quantum paraelectric  $\text{EuTiO}_3$ . *Phys. Rev. B* 64, 054415 (2001).  
17  
18 21. V. Viallet, J.-F. Marucco, J. Saint, M. Herbst-Ghysel, and N. Drago: Structural, magnetic  
19  
20 and electrical properties of a perovskite containing divalent europium  $\text{EuZrO}_3$ . *J. Alloys*  
21  
22 *Compd.* 461, 346 (2008).  
23  
24 22. Y. Zong, K. Fujita, H. Akamatsu, S. Murai, and K. Tanaka: Antiferromagnetism of perovskite  
25  
26  $\text{EuZrO}_3$ . *J. Solid State Chem.* 183, 168 (2010).  
27  
28 23. T. Kolodiaznyi, K. Fujita, L. Wang, Y. Zong, K. Tanaka, Y. Sakka, and E.  
29  
30 Takayama-Muromachi: Magnetodielectric effect in  $\text{EuZrO}_3$ . *Appl. Phys. Lett.* 96, 252901  
31  
32 (2010).  
33  
34 24. C. J. Fennie and K. M. Rabe: Magnetic and electric phase control in epitaxial  $\text{EuTiO}_3$  from  
35  
36 first principles. *Phys. Rev. Lett.* 97, 267602 (2006).  
37  
38 25. R. Ranjan, H. S. Nabi, and R. Pentcheva: Electronic structure and magnetism of  $\text{EuTiO}_3$ : a  
39  
40 first-principles study. *J. Phys.: Condens. Matter* 19, 406217 (2007).  
41  
42 26. H. Akamatsu, Y. Kumagai, F. Oba, K. Fujita, H. Murakami, K. Tanaka, and I. Tanaka:  
43  
44 Antiferromagnetic superexchange via 3d states of titanium in  $\text{EuTiO}_3$  as seen from hybrid  
45  
46 Hartree-Fock density functional calculations. *Phys. Rev. B* 83, 214421 (2011).  
47  
48 27. K. Fujita, N. Wakasugi, S. Murai, Y. Zong, and K. Tanaka: High-quality antiferromagnetic  
49  
50  
51  
52  
53  
54  
55  
56  
57  
58  
59  
60

- 1  
2  
3  
4  
5  
6 EuTiO<sub>3</sub> epitaxial thin films on SrTiO<sub>3</sub> prepared by pulsed laser deposition and  
7  
8 post-annealing. *Appl. Phys. Lett.* 94, 062512 (2009).  
9
- 10  
11 28. J. H. Lee, L. Fang, E. Vlahos, X. Ke, Y. W. Jung, L. Fitting Kourkoutis, J.-W. Kim, P. J.  
12  
13 Ryan, T. Heeg, M. Roeckerath, V. Goian, M. Bernhagen, R. Uecker, P. C. Hammel, K. M.  
14  
15 Rabe, S. Kamba, J. Schubert, J. W. Freeland, D. A. Muller, C. J. Fennie, P. Schiffer, V.  
16  
17 Gopalan, E. Johnston-Halperin, and D. G. Schlom: A strong ferroelectric ferromagnet created  
18  
19 by means of spin–lattice coupling. *Nature* 466, 954 (2010).  
20  
21
- 22  
23 29. H. Akamatsu, K. Fujita, Y. Zong, N. Takemoto, S. Murai, and K. Tanaka: Impact of  
24  
25 amorphization on the magnetic properties of EuO-TiO<sub>2</sub> system. *Phys. Rev. B* 82, 224403  
26  
27 (2010).  
28  
29
- 30  
31 30. Y. Zong, K. Fujita, H. Akamatsu, S. Nakashima, S. Murai, and K. Tanaka: Local structure of  
32  
33 amorphous EuO-TiO<sub>2</sub> thin films probed by x-ray absorption fine structure. *J. Amer. Ceram.*  
34  
35 *Soc.* 95, 716 (2012).  
36
- 37  
38 31. K. S. Takahashi, M. Onoda, M. Kawasaki, N. Nagaosa, and Y. Tokura: Control of the  
39  
40 anomalous Hall effect by doping in Eu<sub>1-x</sub>La<sub>x</sub>TiO<sub>3</sub> thin films. *Phys. Rev. Lett.* 103, 057204  
41  
42 (2009).  
43  
44
- 45  
46 32. P. W. Anderson: New approach to the theory of superexchange interactions. *Phys. Rev.* 115,  
47  
48 2 (1959).  
49
- 50  
51 33. M. W. Shafer: Preparation and crystal chemistry of divalent europium compounds. *J. Appl.*  
52  
53 *Phys.* 36, 1145 (1965).  
54
- 55  
56 34. J. Kunes, W. Ku, and W. E. Pickett: Exchange coupling in Eu monochalcogenides from first  
57  
58 principles. *J. Phys. Soc. Jpn.* 74, 1408 (2005).  
59  
60

- 1  
2  
3  
4  
5  
6 35. N. M. Souza-Neto, D. Haskel, Y.-C. Tseng, and G. Lapertot: Pressure-Induced Electronic  
7  
8 Mixing and Enhancement of Ferromagnetic Ordering in EuX (X=Te, Se, S, O) Magnetic  
9  
10 Semiconductors. *Phys. Rev. Lett.* 102, 057206 (2009).  
11  
12  
13 36. J. Greedan and G. J. McCarthy: Crystal chemistry and magnetic properties of  $\text{Eu}_2\text{TiO}_4$   
14  
15 and  $\text{Eu}_3\text{Ti}_2\text{O}_7$ . *Mater. Res. Bull.* 7, 531 (1972).  
16  
17  
18 37. J. P. Sanchez, J. M. Friedt, R. Horne, and A. J. Van Duyneveldt: Spin glass transition and  
19  
20 hyperfine parameters in  $\text{FeO-Al}_2\text{O}_3\text{-SiO}_2$  glasses: *J. Phys. C: Solid State Phys.* 17, 127  
21  
22 (1984).  
23  
24  
25 38. G. C. Lau, T. Klimczuk, F. Ronning, T. M. McQueen, and R. J. Cava: Magnetic properties  
26  
27 of the garnet and glass forms of  $\text{Mn}_3\text{Al}_2\text{Si}_3\text{O}_{12}$ . *Phys. Rev. B* 80, 214414 (2009).  
28  
29  
30 39. S. Nakamura, S. Soeya, N. Ikeda, and M. Tanaka: Spin-glass behavior in amorphous  
31  
32  $\text{BiFeO}_3$ . *J. Appl. Phys.* 74, 5652 (1993).  
33  
34  
35 40. M. D. Mukadam, S. M. Yusuf, P. Sharma, S. K. Kulshreshtha, and G. K. Dey: Dynamics of  
36  
37 spin clusters in amorphous  $\text{Fe}_2\text{O}_3$ . *Phys. Rev. B* 72, 174408 (2005).  
38  
39  
40 41. H. Akamatsu, K. Tanaka, K. Fujita, and S. Murai: Spin dynamics in  $\text{Fe}_2\text{O}_3\text{-TeO}_2$  glass:  
41  
42 experimental evidence for an amorphous oxide spin glass. *Phys. Rev. B* 74, 012411 (2006).  
43  
44  
45 42. H. Akamatsu, K. Tanaka, K. Fujita, and S. Murai: Spin dynamics in oxide glass of  
46  
47  $\text{Fe}_2\text{O}_3\text{-Bi}_2\text{O}_3\text{-B}_2\text{O}_3$  system. *J. Magn. Magn. Mater.* 310, 1506 (2007).  
48  
49  
50 43. K. Tanaka, H. Akamatsu, S. Nakashima, and K. Fujita: Magnetic properties of disordered  
51  
52 oxides with iron and manganese ions. *J. Non-Cryst. Solids* 354, 1346 (2008).  
53  
54  
55 44. H. Akamatsu, K. Tanaka, K. Fujita, and S. Murai: Magnetic phase transitions in  
56  
57  $\text{Fe}_2\text{O}_3\text{-Bi}_2\text{O}_3\text{-B}_2\text{O}_3$  glasses. *J. Phys.: Condens. Matter* 20, 235216 (2008).  
58  
59  
60

- 1  
2  
3  
4  
5  
6 45. H. Akamatsu, K. Fujita, S. Murai, and K. Tanaka: Magneto-optical properties of transparent  
7  
8 divalent iron phosphate glasses. *Appl. Phys. Lett.* 92, 251908 (2008).  
9  
10  
11 46. H. Akamatsu, S. Oku, K. Fujita, S. Murai, and K. Tanaka: Magnetic properties of  
12  
13 mixed-valence iron phosphate glasses. *Phys. Rev. B* 80, 134408 (2009).  
14  
15  
16 47. V.G. Bhide and M. S. Multani: Mössbauer effect in ferroelectric-antiferromagnetic BiFeO<sub>3</sub>.  
17  
18 *Solid State Commun.* 3, 271 (1965).  
19  
20  
21 48. J. Schoenes, E. Kaldis, W. Thöni, and P. Wachter: Optical, magnetic, and magneto-optical  
22  
23 properties of the europium silicate Glass Eu<sub>0.14</sub>Si<sub>0.31</sub>O<sub>0.55</sub>. *Phys. Stat. Sol. A* 51, 173 (1979).  
24  
25  
26 49. H. Akamatsu, K. Fujita, S. Murai, and K. Tanaka: Ferromagnetic Eu<sup>2+</sup>-based oxide glasses  
27  
28 with reentrant spin glass behavior. *Phys. Rev. B* 81, 014423 (2010).  
29  
30  
31 50. B. T. Matthias, R. M. Bozorth, and J. H. Van Vleck: Ferromagnetic interaction in EuO.  
32  
33 *Phys. Rev. Lett.* 7, 160 (1961).  
34  
35  
36 51. Y. Zong, K. Fujita, H. Akamatsu, S. Murai, and K. Tanaka: Ferromagnetic properties with  
37  
38 reentrant spin-glass behavior in amorphous EuZrO<sub>3</sub> thin film. *Phys. Stat. Sol. C* 8, 3051  
39  
40 (2011).  
41  
42  
43  
44  
45  
46  
47  
48  
49  
50  
51  
52  
53  
54  
55  
56  
57  
58  
59  
60

1  
2  
3  
4  
5  
6 Table 1 Molar ratio of Eu to Ti in the as-deposited europium titanate thin films grown on  
7  
8 different sorts of substrate. The molar ratio is almost equal to 1 in all the thin films, suggesting  
9  
10 that stoichiometric  $\text{EuTiO}_3$  was synthesized.  
11  
12  
13  
14

Substrate	Molar ratio of Eu to Ti in the europium titanate thin films
$\text{LaAlO}_3$	1.02
$\text{SrTiO}_3$	0.98
$\text{DyScO}_3$	1.02

For Peer Review

15  
16  
17  
18  
19  
20  
21  
22  
23  
24  
25  
26  
27  
28  
29  
30  
31  
32  
33  
34  
35  
36  
37  
38  
39  
40  
41  
42  
43  
44  
45  
46  
47  
48  
49  
50  
51  
52  
53  
54  
55  
56  
57  
58  
59  
60

Table 2 Variation in lattice constant and lattice volume for  $\text{EuTiO}_3$  thin films grown on  $\text{LaAlO}_3$ ,  $\text{SrTiO}_3$ , and  $\text{DyScO}_3$  substrates. A relative difference in the values between the thin film and bulk  $\text{EuTiO}_3$  is listed.  $\Delta l_1$  and  $\Delta l_2$  denote the change in lattice constant in a direction parallel and perpendicular to the surface of the thin film, respectively.  $\Delta V$  stands for the change in lattice volume relative to the bulk  $\text{EuTiO}_3$ .

Substrate	$\Delta l_1$ (%)	$\Delta l_2$ (%)	$\Delta V$ (%)
$\text{LaAlO}_3$	-0.5	+1.89	+1.56
$\text{SrTiO}_3$	0.0	+2.41	+2.41
$\text{DyScO}_3$	+1.05	+1.77	+3.92

Table 3 Structural parameters obtained from EXAFS for  $\text{Eu}^{2+}$  in amorphous  $\text{EuTiO}_3$  (a-ETO) and  $\text{Eu}_2\text{TiO}_4$  (a-2ETO) thin films.  $n_{\text{Eu}^{2+}}$  and  $d_{\text{Eu-O}}$  denote the average coordination number of  $\text{Eu}^{2+}$  and the nearest-neighboring Eu–O bond length, respectively.

Compound	$n_{\text{Eu}^{2+}}$	$d_{\text{Eu-O}}$ (nm)
amorphous $\text{EuTiO}_3$	6.4	0.2480
amorphous $\text{Eu}_2\text{TiO}_4$	6.3	0.2472

## Figure captions

Fig. 1 AFM images of  $\text{EuTiO}_3$  thin films grown on (a)  $\text{LaAlO}_3$ , (b)  $\text{SrTiO}_3$ , and (c)  $\text{DyScO}_3$  substrates. LAO, STO, and DSO denote  $\text{LaAlO}_3$ ,  $\text{SrTiO}_3$ , and  $\text{DyScO}_3$ , respectively.

Fig. 2 Reciprocal space mappings for  $\text{EuTiO}_3$  thin films as well as  $\text{LaAlO}_3$ ,  $\text{SrTiO}_3$ , and  $\text{DyScO}_3$  substrates.  $Q_x$  and  $Q_y$  correspond to the reciprocal lattice vectors parallel and perpendicular to the surface of the  $\text{EuTiO}_3$  thin film, respectively. The small circle shown in each of the mappings denotes the reciprocal lattice of bulk  $\text{EuTiO}_3$ .

Fig. 3 Dependence of magnetization on temperature for  $\text{EuTiO}_3$  thin films grown on  $\text{LaAlO}_3$  (diamond),  $\text{SrTiO}_3$  (circle), and  $\text{DyScO}_3$  (square) substrates as well as for bulk  $\text{EuTiO}_3$  (triangle). The inset is a magnified view for bulk  $\text{EuTiO}_3$ .

Fig. 4 Dependence of magnetization on magnetic field at 2 K for  $\text{EuTiO}_3$  thin films grown on  $\text{LaAlO}_3$  (diamond),  $\text{SrTiO}_3$  (circle), and  $\text{DyScO}_3$  (square) substrates as well as for bulk  $\text{EuTiO}_3$  (triangle). The insets depict the magnetization at low magnetic fields for  $\text{EuTiO}_3$  thin film grown on  $\text{SrTiO}_3$  substrate (right inset: circle) and for bulk  $\text{EuTiO}_3$  (left inset: triangle).

Fig. 5 Magnetic configurations and magnetic interactions in  $\text{EuTiO}_3$  lattice. A, F, and G denote A-type antiferromagnetic, ferromagnetic, and G-type antiferromagnetic states, respectively.  $J_1$  and  $J_2$  stand for the exchange coupling constant between nearest-neighboring

1  
2  
3  
4  
5  
6 and next-nearest-neighboring  $\text{Eu}^{2+}$  ions, respectively.  
7  
8  
9

10 Fig. 6 Mechanism of indirect exchange interaction between  $\text{Eu}^{2+}$  ions to lead to ferromagnetic  
11 state. 4f spins interact ferromagnetically with each other via 5d state.  
12  
13  
14  
15  
16  
17

18 Fig. 7 (a) X-ray diffraction patterns for amorphous  $\text{EuTiO}_3$  (a-ETO) and  $\text{Eu}_2\text{TiO}_4$  (a-2ETO) thin  
19 films. (b) high-resolution transmission electron micrograph and selected area electron  
20 diffraction pattern for amorphous  $\text{EuTiO}_3$ .  
21  
22  
23  
24  
25  
26

27 Fig. 8 Dependence of magnetization on temperature at a applied dc magnetic field of 100 Oe  
28 for amorphous  $\text{EuTiO}_3$  (a-ETO) and  $\text{Eu}_2\text{TiO}_4$  (a-2ETO) thin films. The arrows indicate an  
29 inflection point in each of the magnetization curves. The Curie temperature is defined as the  
30 temperature giving the inflection point.  
31  
32  
33  
34  
35  
36  
37  
38  
39

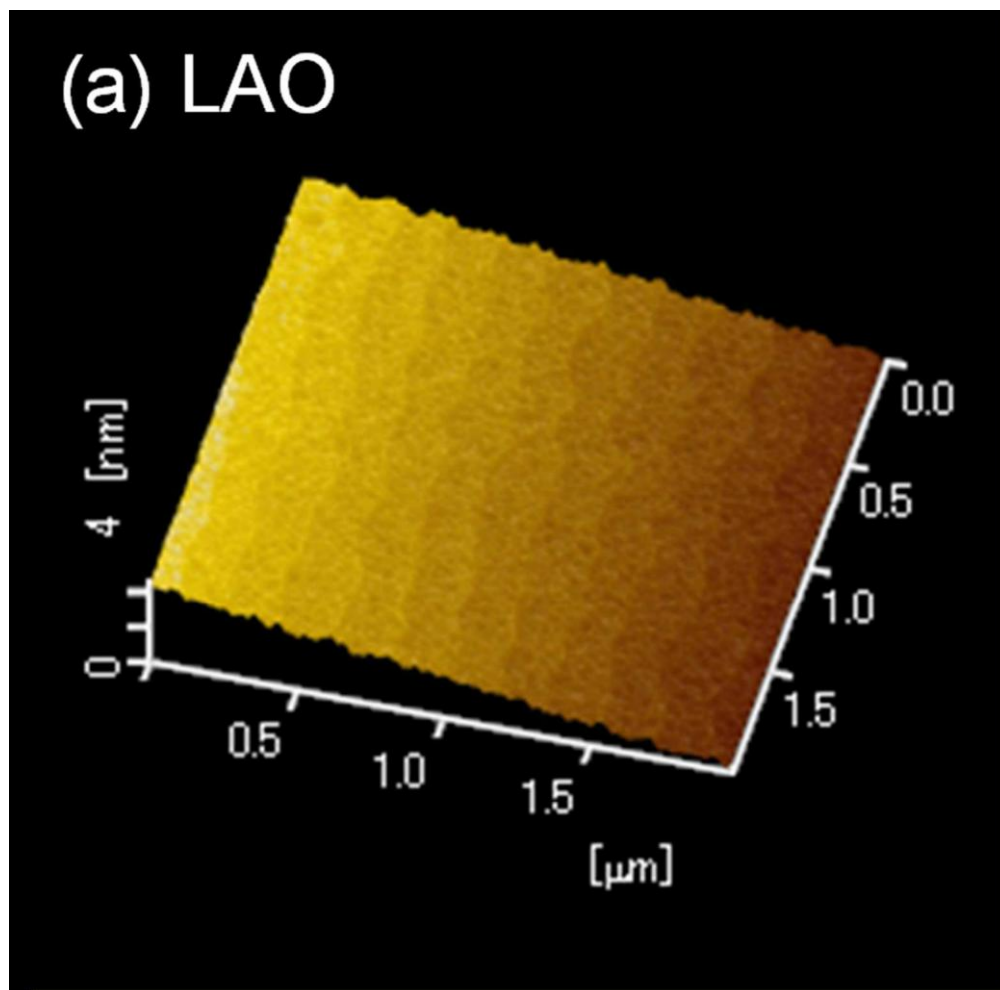
40 Fig. 9 Dependence of magnetization on magnetic field at 2.0 K for amorphous  $\text{EuTiO}_3$   
41 (a-ETO) and  $\text{Eu}_2\text{TiO}_4$  (a-2ETO) thin films. The solid curve represents the theoretical one  
42 calculated using the Brillouin function for paramagnetic  $\text{Eu}^{2+}$  ions at 2.0 K  
43  
44  
45  
46  
47  
48

49 Fig. 10 Eu  $L_3$ -edge EXAFS spectra in R-space (open squares) and theoretical curves (solid  
50 lines) fitted to the first-shell components of the experimental data for (a)  $\text{EuTiO}_3$  (a-ETO) and  
51 (b)  $\text{Eu}_2\text{TiO}_4$  (a-2ETO) thin films. R is the radial distance from Eu and  $\chi(R)$  is the EXAFS  
52 oscillation curve. The insets illustrate a comparison of the real part of Fourier filtered  
53  
54  
55  
56  
57  
58  
59  
60

1  
2  
3  
4  
5  
6  
7  
8  
9  
10  
11  
12  
13  
14  
15  
16  
17  
18  
19  
20  
21  
22  
23  
24  
25  
26  
27  
28  
29  
30  
31  
32  
33  
34  
35  
36  
37  
38  
39  
40  
41  
42  
43  
44  
45  
46  
47  
48  
49  
50  
51  
52  
53  
54  
55  
56  
57  
58  
59  
60

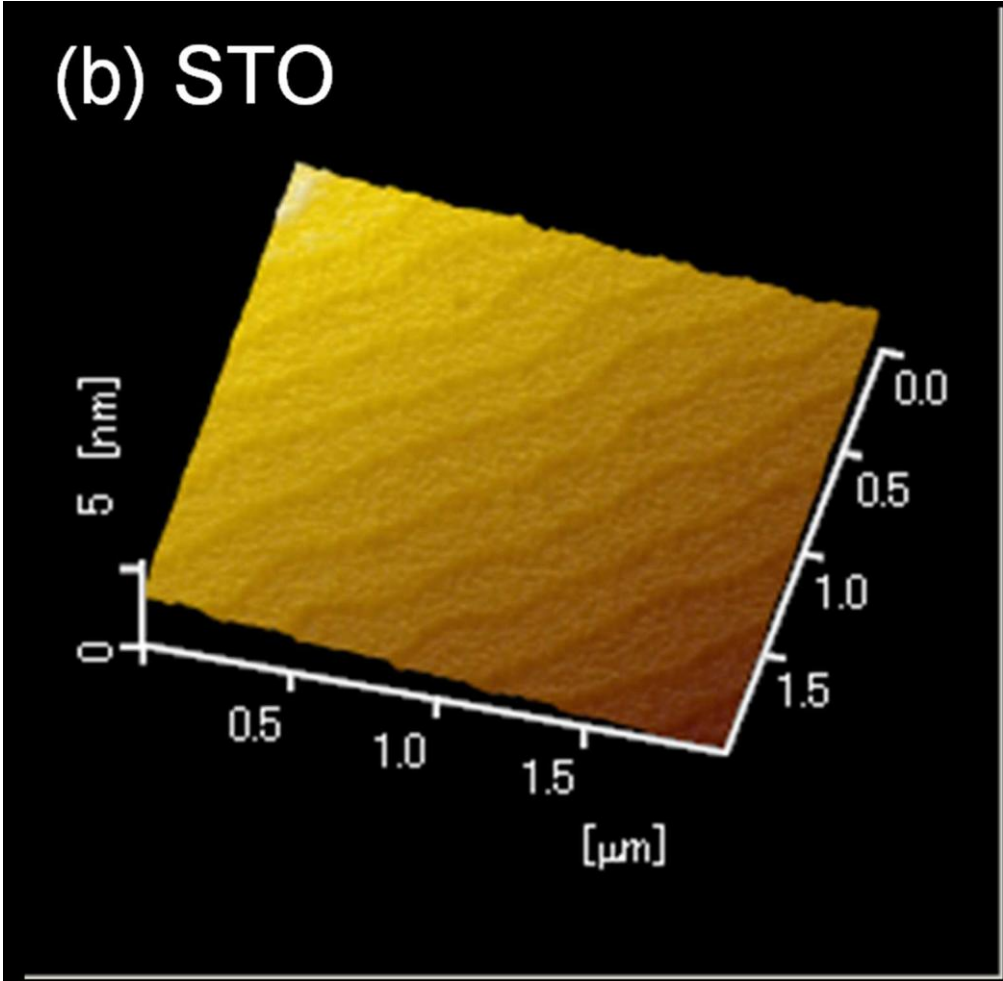
first-shell signals in q-space (open squares) and the theoretical curves (sold lines).

For Peer Review

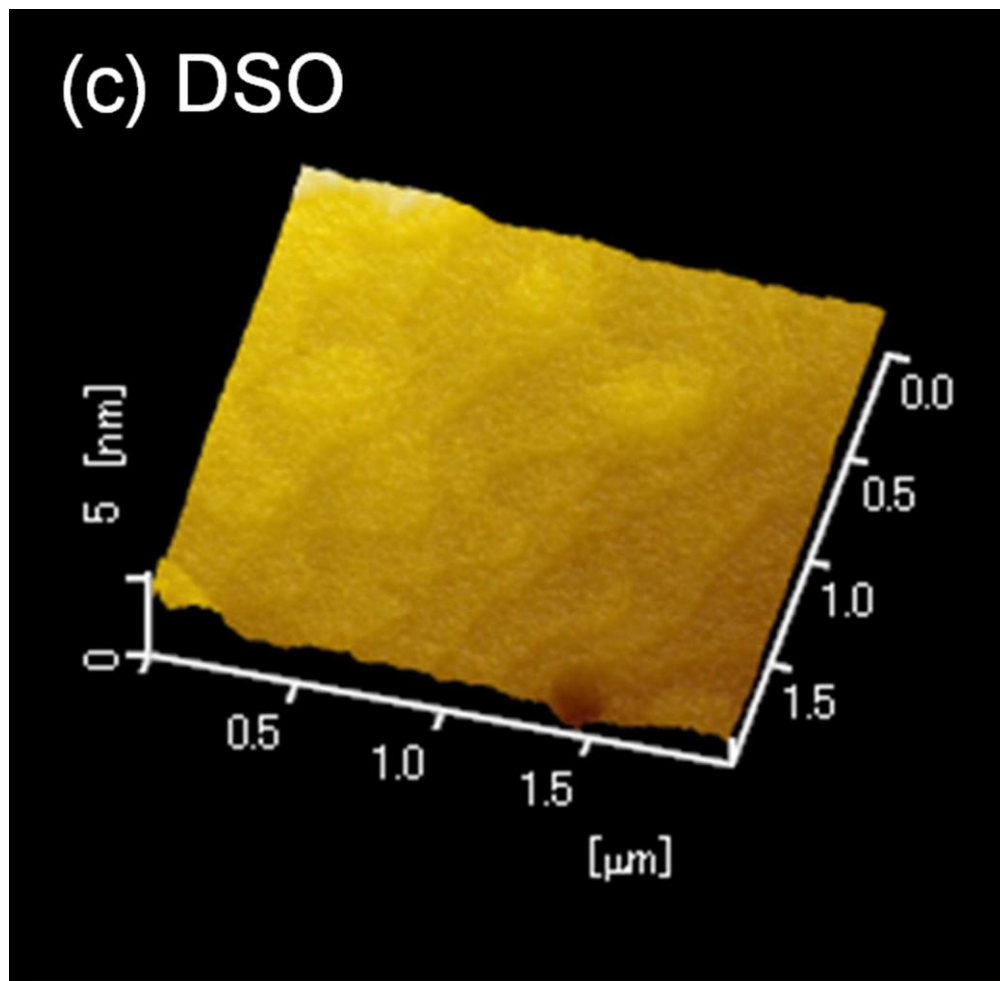


123x121mm (150 x 150 DPI)

1  
2  
3  
4  
5  
6  
7  
8  
9  
10  
11  
12  
13  
14  
15  
16  
17  
18  
19  
20  
21  
22  
23  
24  
25  
26  
27  
28  
29  
30  
31  
32  
33  
34  
35  
36  
37  
38  
39  
40  
41  
42  
43  
44  
45  
46  
47  
48  
49  
50  
51  
52  
53  
54  
55  
56  
57  
58  
59  
60

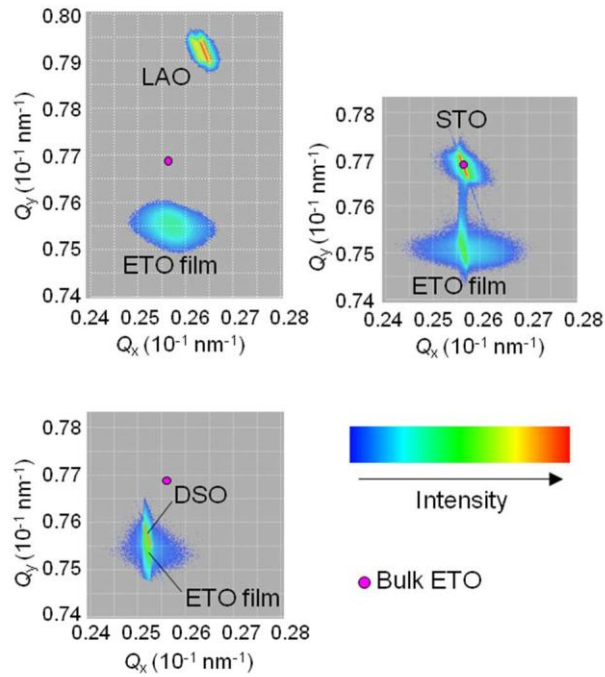


122x120mm (150 x 150 DPI)



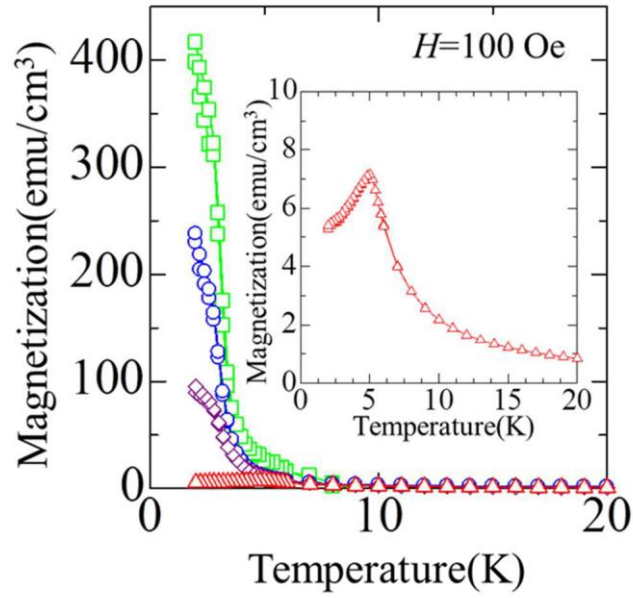
122x120mm (150 x 150 DPI)

1  
2  
3  
4  
5  
6  
7  
8  
9  
10  
11  
12  
13  
14  
15  
16  
17  
18  
19  
20  
21  
22  
23  
24  
25  
26  
27  
28  
29  
30  
31  
32  
33  
34  
35  
36  
37  
38  
39  
40  
41  
42  
43  
44  
45  
46  
47  
48  
49  
50  
51  
52  
53  
54  
55  
56  
57  
58  
59  
60



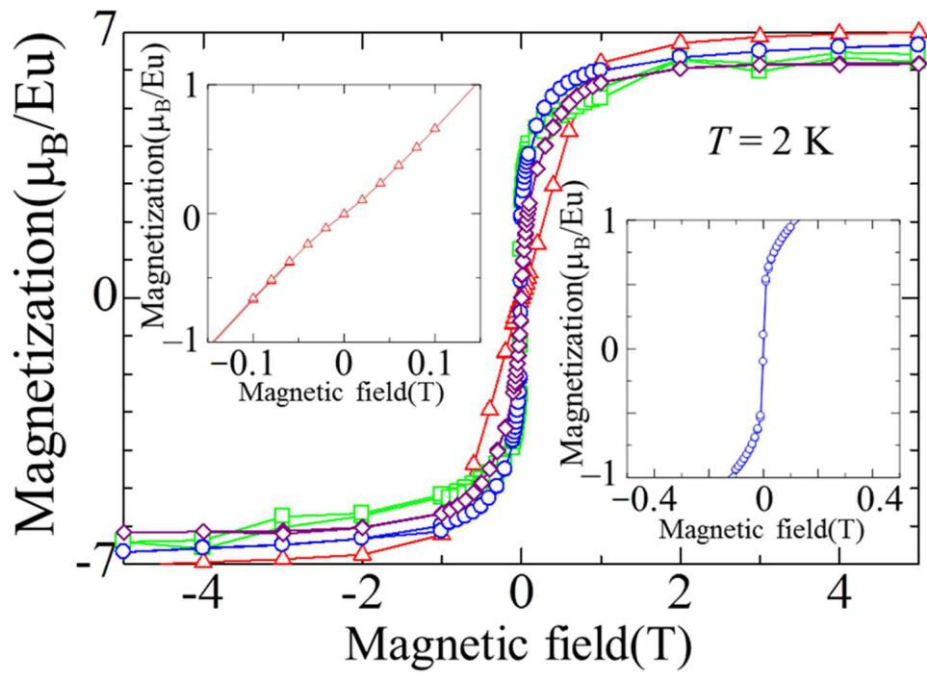
254x190mm (96 x 96 DPI)

Review



254x190mm (96 x 96 DPI)

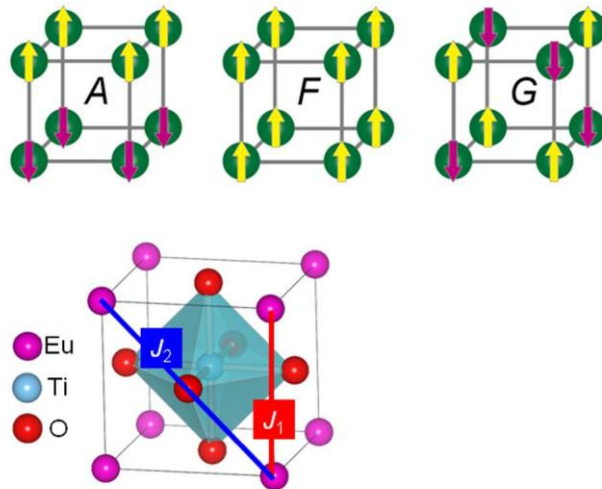
Review



254x190mm (96 x 96 DPI)

Review

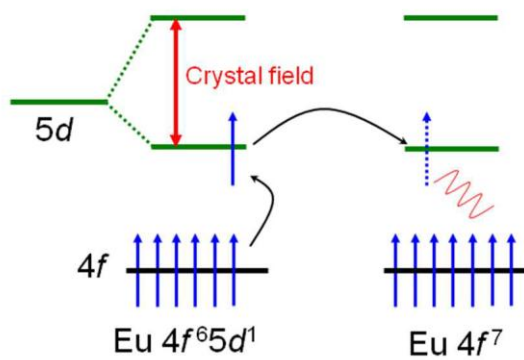
1  
2  
3  
4  
5  
6  
7  
8  
9  
10  
11  
12  
13  
14  
15  
16  
17  
18  
19  
20  
21  
22  
23  
24  
25  
26  
27  
28  
29  
30  
31  
32  
33  
34  
35  
36  
37  
38  
39  
40  
41  
42  
43  
44  
45  
46  
47  
48  
49  
50  
51  
52  
53  
54  
55  
56  
57  
58  
59  
60



254x190mm (96 x 96 DPI)

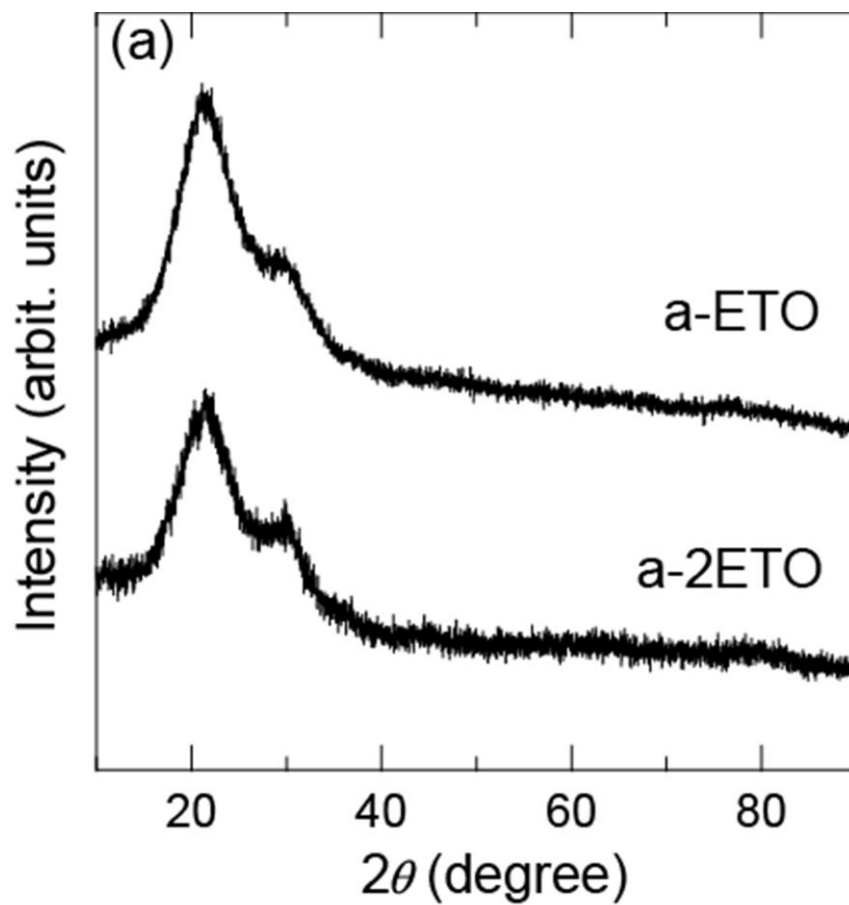
Review

1  
2  
3  
4  
5  
6  
7  
8  
9  
10  
11  
12  
13  
14  
15  
16  
17  
18  
19  
20  
21  
22  
23  
24  
25  
26  
27  
28  
29  
30  
31  
32  
33  
34  
35  
36  
37  
38  
39  
40  
41  
42  
43  
44  
45  
46  
47  
48  
49  
50  
51  
52  
53  
54  
55  
56  
57  
58  
59  
60



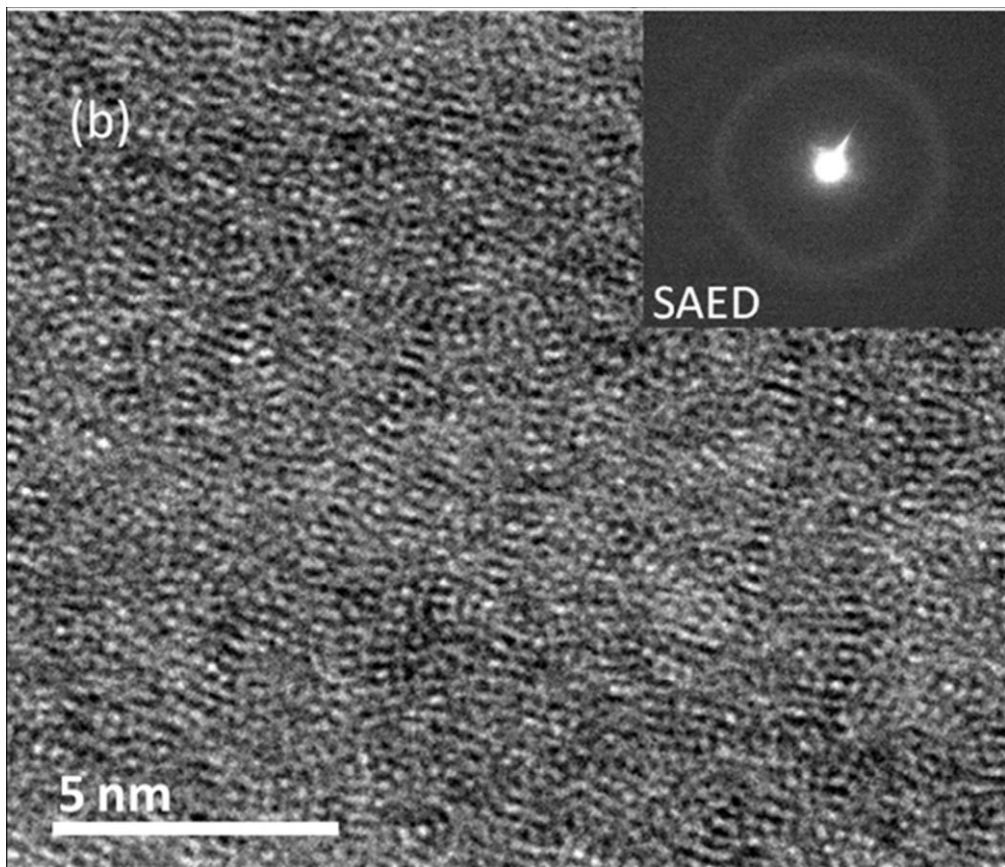
254x190mm (96 x 96 DPI)

Review

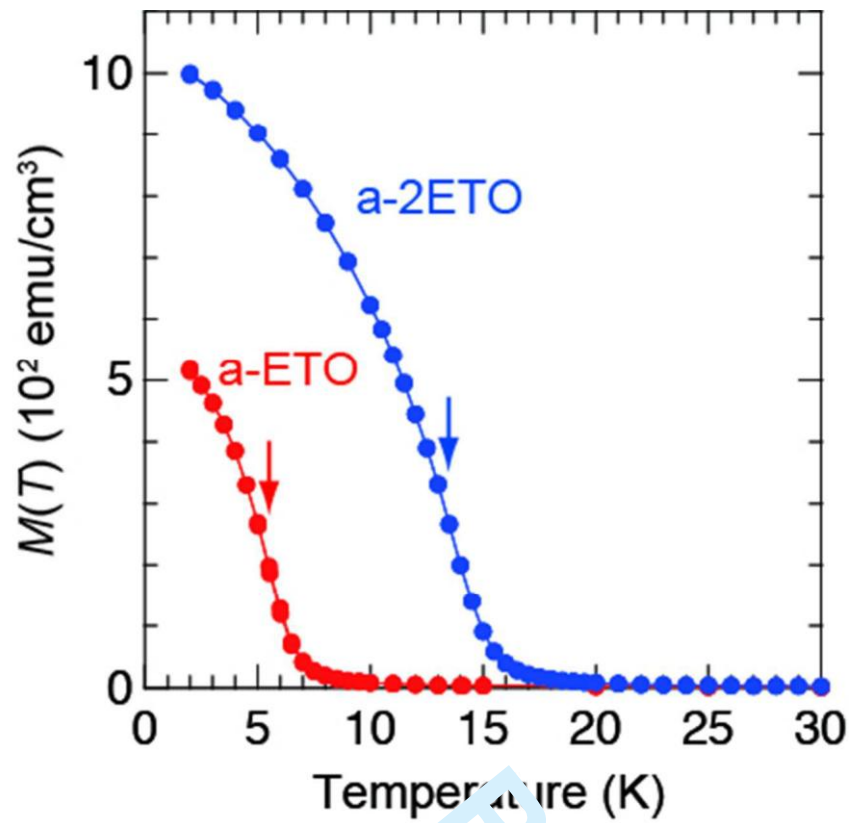


149x159mm (72 x 72 DPI)

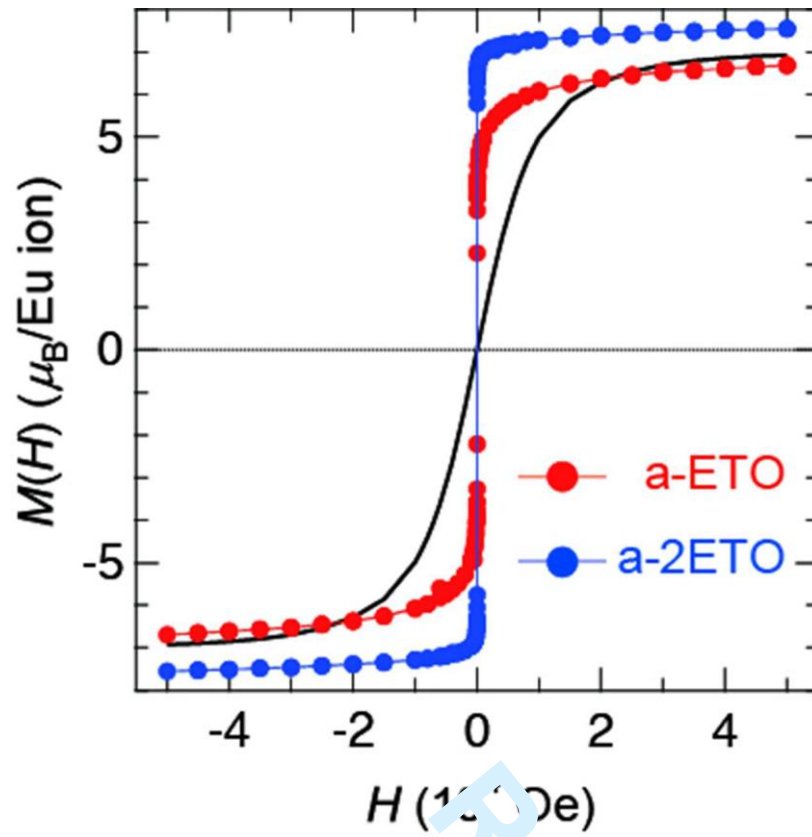
1  
2  
3  
4  
5  
6  
7  
8  
9  
10  
11  
12  
13  
14  
15  
16  
17  
18  
19  
20  
21  
22  
23  
24  
25  
26  
27  
28  
29  
30  
31  
32  
33  
34  
35  
36  
37  
38  
39  
40  
41  
42  
43  
44  
45  
46  
47  
48  
49  
50  
51  
52  
53  
54  
55  
56  
57  
58  
59  
60



102x88mm (150 x 150 DPI)



149x143mm (72 x 72 DPI)



142x146mm (72 x 72 DPI)

Review

1  
2  
3  
4  
5  
6  
7  
8  
9  
10  
11  
12  
13  
14  
15  
16  
17  
18  
19  
20  
21  
22  
23  
24  
25  
26  
27  
28  
29  
30  
31  
32  
33  
34  
35  
36  
37  
38  
39  
40  
41  
42  
43  
44  
45  
46  
47  
48  
49  
50  
51  
52  
53  
54  
55  
56  
57  
58  
59  
60

